X-684-77-202
PREPRINT

TMX 71379

IMPULSIVE SOLAR X-RAY BURSTS

CAROL JO CRANNELL
KENNETH J. FROST
CHRISTIAN MÄTZLER
KENICHIRO OHKI
JACK L. SABA

AUGUST 1977

GSFC

GODDARD SPACE FLIGHT CENTER
GREENBELT, MARYLAND

X-684-77-202
Preprint

IMPULSIVE SOLAR X-RAY BURSTS

Carol Jo Crannell
Kenneth J. Frost
Christian Mätzler*
Kenichiro Ohki**
Jack L. Saba***

August 1977

*Swiss National Science Foundation Fellow.
**NAS-NRC Research Fellow.
***Computer Sciences Corporation.

GODDARD SPACE FLIGHT CENTER
Greenbelt, Maryland

IMPULSIVE SOLAR X-RAY BURSTS

Carol Jo Crannell
Kenneth J. Frost
Christian Mätzler*
Kenichiro Ohki**
Jack L. Saba***

ABSTRACT

A set of 22 simple, impulsive solar flares, identified in the OSO-5 hard X-ray data, have been analyzed together with coincident microwave and meterwave radio observations. The rise times and fall times of the X-ray bursts are found to be highly correlated and effectively equal, strongly suggesting a flare energizing mechanism that is reversible. The good time resolution available for these observations reveals that the microwave emission is influenced by an additional process, evident in the tendency of the microwave emission to peak later and decay more slowly than the symmetric X-ray bursts. Meterwave emission is observed in coincidence with the 5 events which show the strongest time correlation between the X-ray and microwave burst structure. This meterwave emission is characterized by U-burst radiation, indicating confinement of the flare source. The relationship found between the X-ray burst duration and the calculated flare diameter, together with the thermal character of the X-ray spectra, gives additional support to the hypothesis that these flares are driven by adiabatic compression and expansion of a magnetically confined plasma which is the common, primary source of both X-ray and microwave emission.

*Swiss National Science Foundation Fellow.
**NAS-NRC Research Fellow.
***Computer Sciences Corporation.

CONTENTS

ILLUSTRATIONS

ILLUSTRATIONS (Continued)

TABLES

IMPULSIVE SOLAR X-RAY BURSTS

1. INTRODUCTION

X rays from electron bremsstrahlung and microwaves from synchrotron radiation provide the most direct evidence of the role of energetic electrons in solar flares. Studies of these emissions are motivated by the fact that answers to some of the most fundamental questions concerning solar flares remain uncertain (Kahler 1971, Craig and Brown 1976, and Korchak 1976). In particular, a number of competitive models have been invoked to explain how flare particles are energized (Kahler 1975, Benz 1977, Hoyng 1977, and Spicer 1977). High-energy X rays and microwave emission have shown evidence of significant temporal correlations and of the most rapid time structure observed in any primary solar flare phenomenon (Frost 1969, Kane and Anderson 1970, Flückiger 1973, and Hoyng et al. 1976), suggesting their common origin and detailed association with fundamental processes during solar flares.

The characteristics exhibited by high-energy X-ray emission encompass temporal structure ranging from variations of order one second, the limiting time resolution of current instrumentation, to durations of order one hour; peak intensities ranging more than three orders of magnitude in absolute flux; and spectra with a wide range of slopes and temporal variations (Peterson and Winckler 1959, Kane and Anderson 1970, Frost and Dennis 1971, Kane 1974, Datlowe et al. 1974, and van Beek et al. 1974). Some complex bursts exhibit nearly the full range of these characteristics within a single event. The impulsive phase is characterized by a rapid rise and fall of both the X-ray and the microwave flux and by an X-ray spectrum which decreases much more steeply for X-ray energies above 100 keV than for energies below that value. Most events exhibit multiply impulsive structure which may or may not be clearly separated in time.

The specific work reported here was motivated by a desire to understand the dynamics of impulsive solar phenomena. The observations of high-energy X-rays from solar flares obtained with OSO-5 include a number of events which appear to be *purely impulsive* with an uncomplicated time structure consisting of a single rise and fall. A study of these simple impulsive events, together with associated emission at other wavelengths, was undertaken to determine the properties of such bursts. Restricting the present investigation to a homogeneous set of the simplest events reduces the number of physical process which must be treated simultaneously, thereby improving the probability of finding a satisfactory model. This work may lead to an understanding of more complex solar flares as an agglomeration of a number of impulsive spikes.

The most striking characteristic of the events selected for study is the symmetry between the rise and fall of the hard X-ray emission. Perhaps because this feature has not been noted previously, symmetry (i.e., reversibility) is not an inherent characteristic of the models which are commonly accepted to describe hard X-ray emission in solar flares. The beaming and trapping models summarized by Kane (1974) and the asymmetric magnetic-field model more recently suggested by Mätzler (1976) all predict rise times governed by the mechanisms which accelerate and inject solar flare electrons into the emission region. For the models based on continuous injection (Hudson 1972, Kane 1973, and Mätzler 1976), fall times are governed by the same acceleration and injection mechanisms that determine the rise. For models based on impulsive injection (Takakura 1973), electron injection ends at the time of peak X-ray emission so that the fall time is determined by other processes such as electron leakage and energy loss. Only if the processes which govern the rise of the burst are the same as those which govern the fall can symmetry be a natural consequence of the model. No acceleration or energizing process which is inherently reversible with respect to the time of peak emission has been suggested in conjunction with the emission models based on continuous injection.

Because the symmetry between the rise and fall of the X-ray emission is such a significant property of the impulsive events selected for the present study, the analysis of these events has been based on the simplest energizing mechanism for which the symmetric rise and fall is a natural consequence. That process is an adiabatic compression followed by an adiabatic expansion of the solar flare plasma. In the same spirit of simplicity, the X-ray and microwave emissions are assumed to originate from a common thermal population of electrons. Throughout the present work, these assumptions are tested by comparisons of the observations with implications of the assumed physical mechanisms. The relationships among the observations and the derived flare parameters are found to be consistent with the hypothesis that these impulsive flares are energized by an adiabatic compression of the source region which is the primary origin of both X-ray and microwave radiation. The model is developed in more detail by Mätzler et al. (1977), hereinafter referred to as Paper 2.

In the next section, the selection criteria for the set of 22 impulsive spike bursts are described and the observational data for these events are presented. Physical parameters derived from these observations and the relationships between the various parameters are presented in Section 3. In Section 4, the significance of the flare parameters is discussed in light of instrumental and analytic effects and characteristics of the impulsive flare process. The conclusions are summarized in Section 5.

2. PRESENTATION OF OBSERVATIONAL DATA

A set of simple impulsive spike bursts was identified in the OSO-5 observations. Because the coverage of these events was not uniform at other wavelengths and because consistency in the selection criteria was desired, all criteria were based solely on the X-ray data. The process of selection was, itself, iterative. All events which exhibited multiple-spike structure were rejected. Similarly, all events which underwent a transition from a rapidly increasing or decreasing flux to a significantly more gradual rise or fall were rejected. Then the accepted events were re-examined to establish more quantitative criteria for selecting the set of events to be analyzed. Each event was ultimately required to satisfy the following criteria: peak counting rate greater than 250 counts s^{-1}; deviations from a monotonic increase followed by a monotonic decrease in the observed counting rates not greater than ±15% of the peak flux of that burst; and approximately continuous time derivatives of the counting rates during the rise and during the fall of each burst. All of the OSO-5 data were re-examined with respect to these criteria. In the final selection twenty-two events were found to satisfy these requirements and so were chosen for analysis as *spike bursts*. *Solar-Geophysical Data* Prompt and Comprehensive Reports (1969 through 1972) were searched for meterwave, microwave, and Hα observations in coincidence with the spike bursts. Data records of the coincident radio events were requested from the reporting observatories.

2.1. X-Ray Observations

The OSO-5 hard X-ray spectrometer sampled the solar flux for a 0.2-second interval every 2 seconds. For each interval, the events detected in the energy range from 14 to 254 keV were analyzed and recorded in nine approximately linearly-spaced energy channels. With the exception of Channel 1, which was 14 keV wide and had a detection efficiency of $\lesssim 0.4\%$, each of the channels was approximately 28 keV wide and had a detection efficiency between 50 and 98% as presented in Table 1. The energy resolution of the detector is given by the expression

$$\Delta E \approx 6\, E^{1/2}, \qquad (1)$$

where ΔE is the FWHM of the Gaussian resolution function of the detector for a photon of energy E, both in keV (B. R. Dennis, private communication). Thus, at 60 keV, ΔE = 46 keV. Further details of the operating properties of the instrument are described by Frost, Dennis, and Lencho (1971).

The temporal profiles of the hard X ray spike bursts observed with OSO-5 are presented in Figures 1-22, arranged in chronological order. The traces labeled

Table 1

Parameters for the OSO-5 X-Ray Spectrometer

Channel Number	Energy Range in keV	Mean Energy in keV	Conversion Factors*	
			Pre	Post
1	14-28	22	9.70×10^{-2}	3.71×10^{-1}
2	28-55	38	1.19×10^{-3}	1.31×10^{-3}
3	55-82	65	7.42×10^{-4}	7.42×10^{-4}
4	82-111	93	6.34×10^{-4}	6.34×10^{-4}
5	111-141	122	6.00×10^{-4}	6.00×10^{-4}
6	141-168	151	6.96×10^{-4}	6.96×10^{-4}
7	168-200	179	6.41×10^{-4}	6.41×10^{-4}
8	200-225	210	8.94×10^{-4}	8.94×10^{-4}
9	225-254	236	8.23×10^{-4}	8.23×10^{-4}

*These are the area-efficiency conversion factors for the periods pre and post 1969 October 26. When multiplied by the counts per second observed in a given channel, they yield the incident flux in units of photons cm^{-2} s^{-1} keV^{-1}.

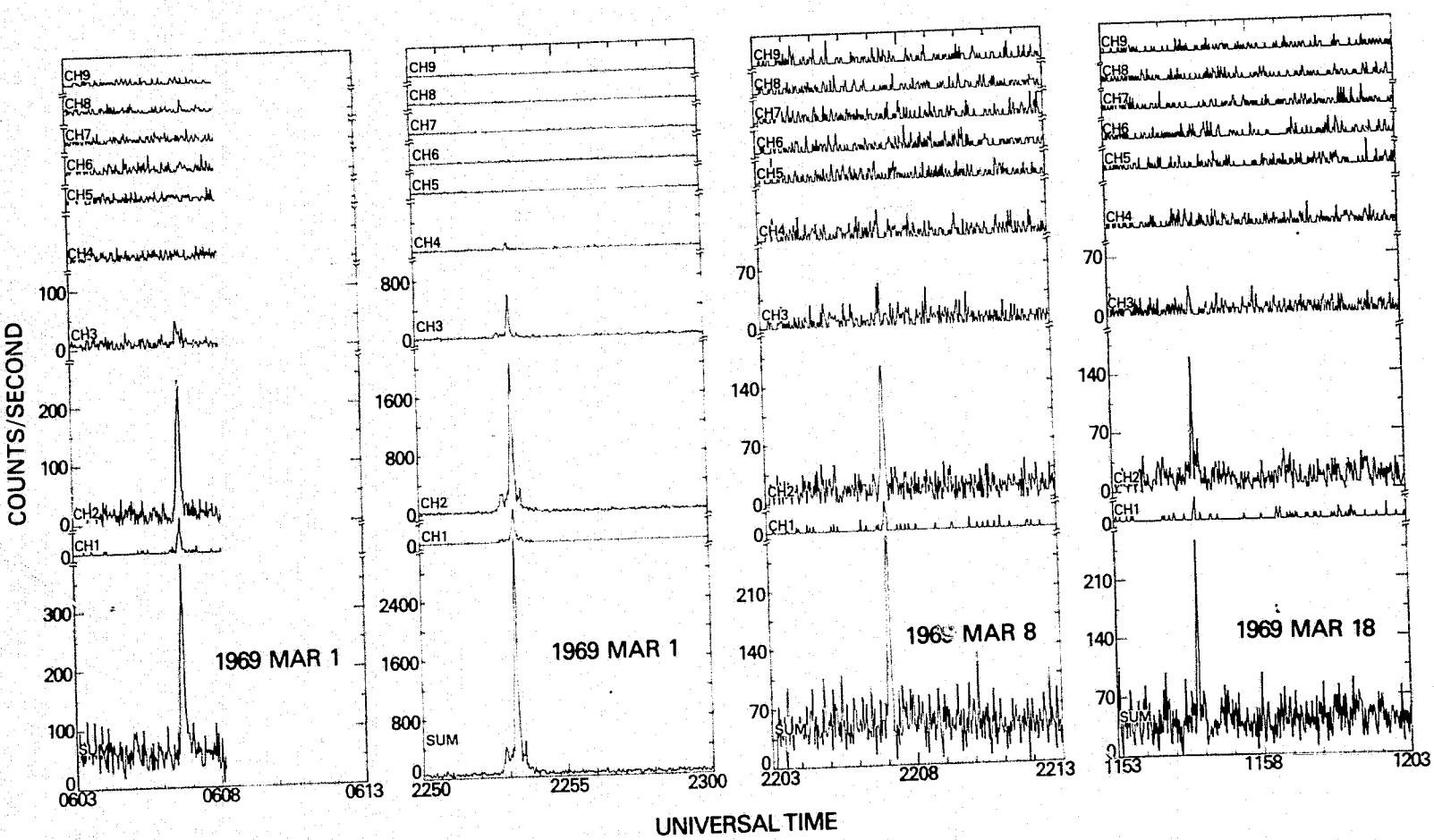

Figures 1-4. Time studies of the observed hard X-ray counting rates.

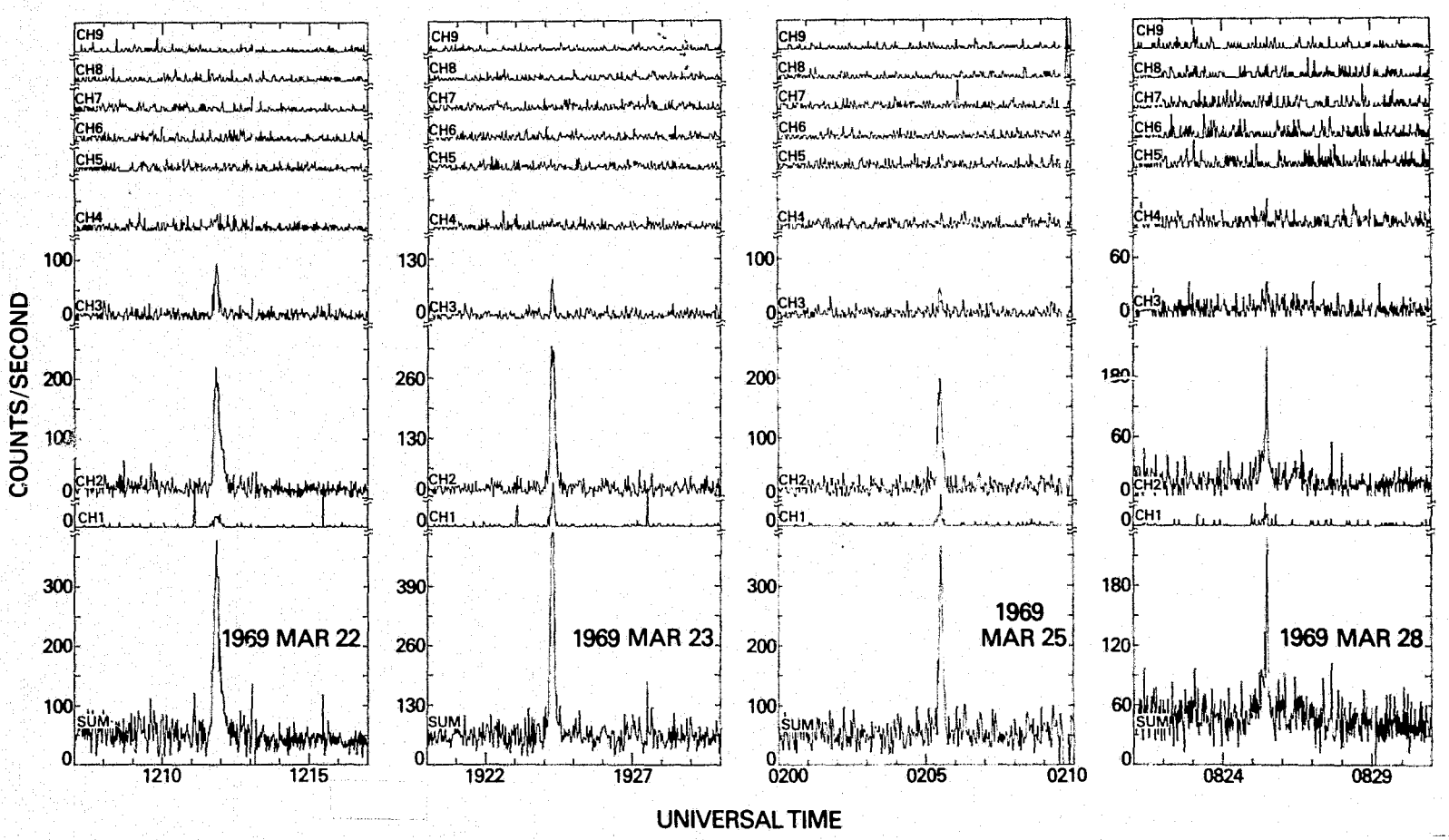

Figures 5-8. Time studies of the observed hard X-ray counting rates.

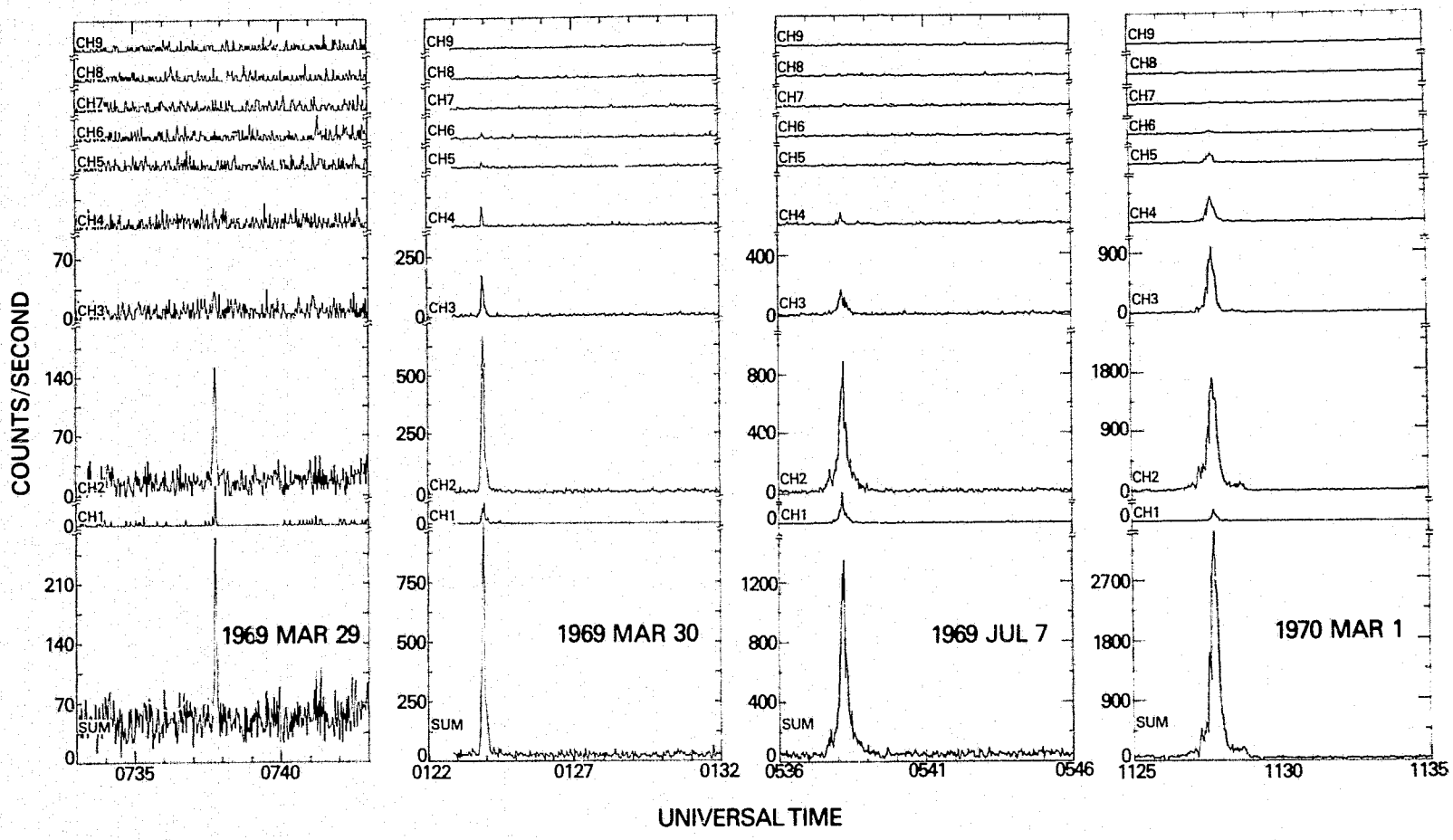

Figures 9-12. Time studies of the observed hard X-ray counting rates.

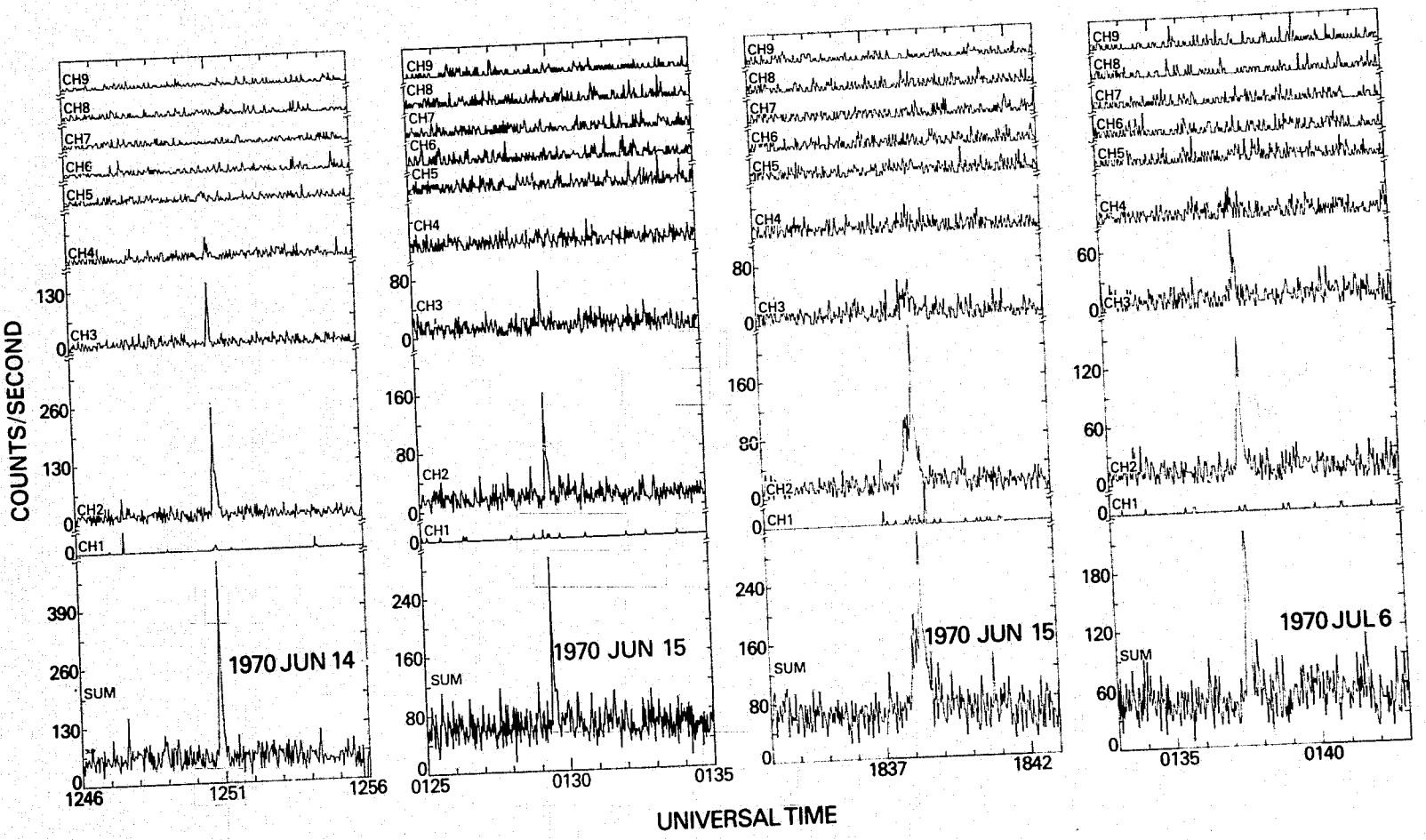

Figures 13-16. Time studies of the observed hard X-ray counting rates.

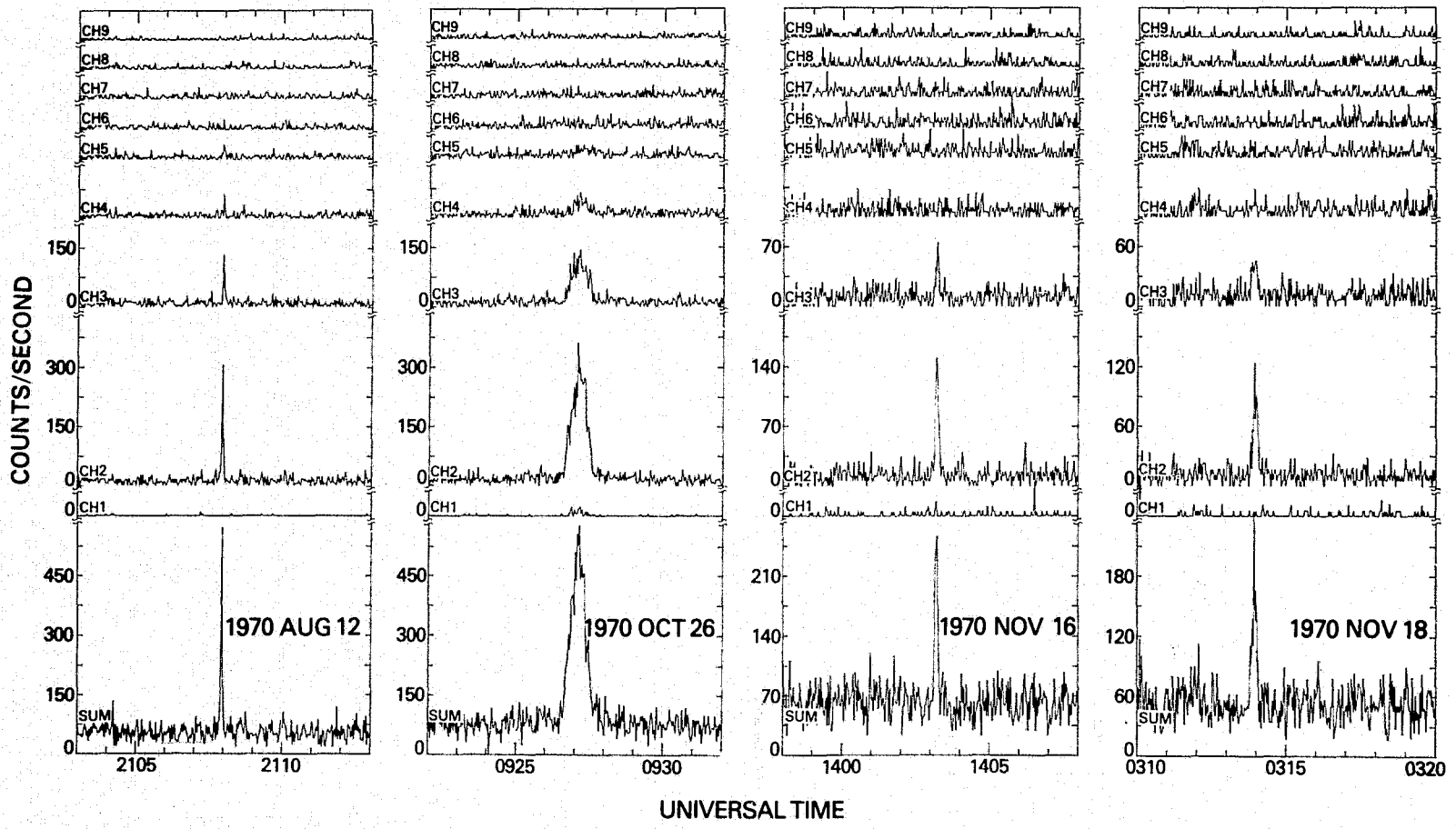

Figures 17-20. Time studies of the observed hard X-ray counting rates.

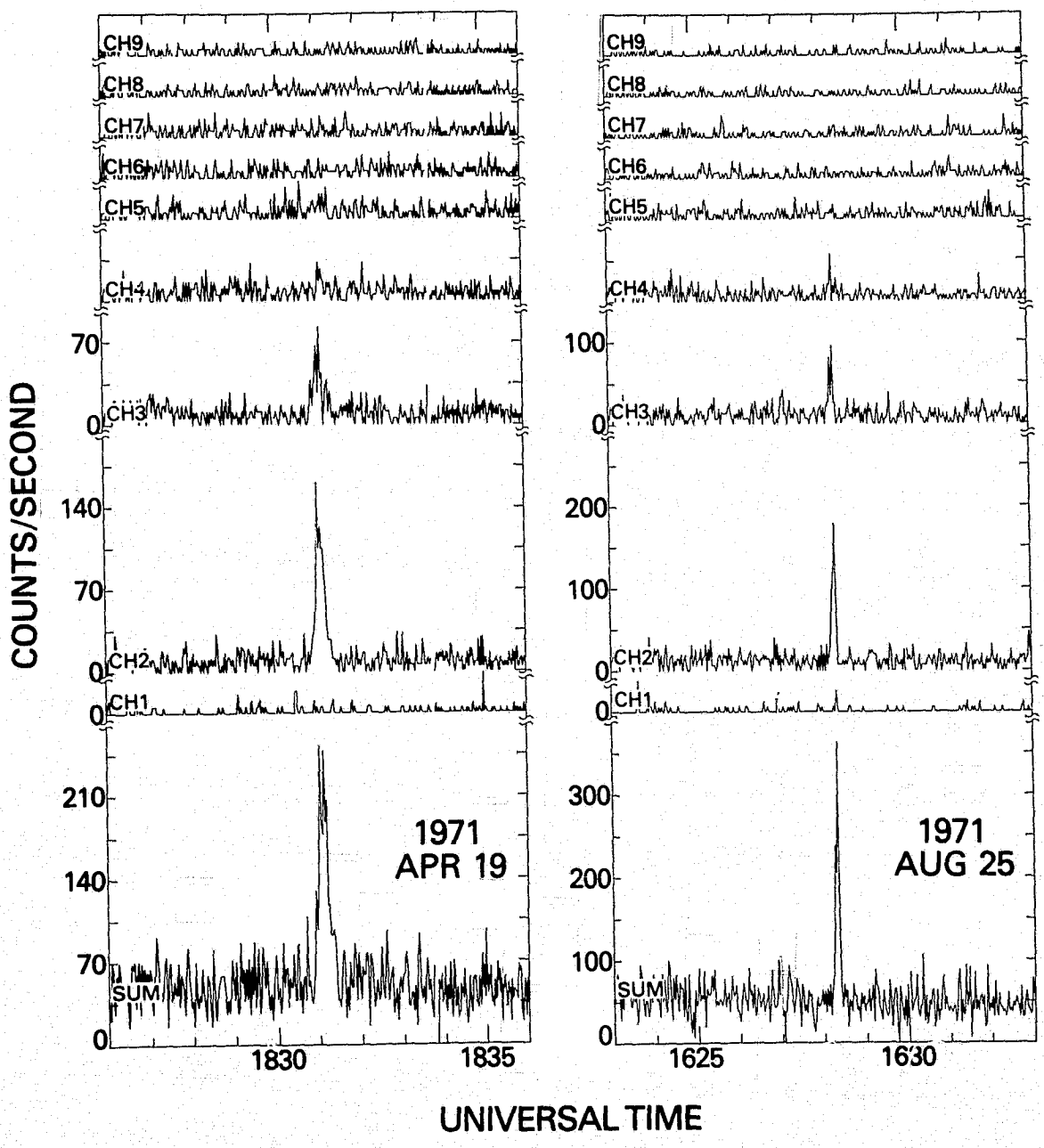

Figures 21-22. Time studies of the observed hard X-ray counting rates.

SUM display the total counting rate of the instrument in the energy range 14 to 254 keV; the traces labeled CH1 through CH9 display the counting rates in each of the nine energy channels. The flare-associated hard X-ray flux was found by subtracting the background flux from the flux observed during the flare. The background was usually computed as the average counting rate over the 10-minute interval immediately preceding the event. When this was not possible, a period following the event was employed. The digital representation of these records comprise the data base from which all the parameters describing the hard X-ray characteristics of the spike bursts were derived.

2.2. Microwave Observations

Coincident meterwave and microwave records were collected for each of the events for which such data were available. Of the twenty-two spike bursts, five were accompanied by meterwave emission and twenty by microwave emission. In Figures 23-27, the temporal profiles of the microwave radiation at frequencies $\gtrsim 10$ GHz are shown together with the corresponding X-ray emission in the energy range 28 to 82 keV for five representative spike bursts.

A summary of all the combined X-ray and microwave time studies for which detailed microwave records were obtained is shown schematically in Figure 28. Each of these seventeen events is represented by a numbered illustration. The event numbers coincide with the figure numbers of the appropriate X-ray profiles and are given in Table 2. The five events annotated with the letter "m" are those observed also at meterwave frequencies. The upper or "V" portion of each illustration depicts the rise, peak, and fall of the hard X-ray emission relative to the microwave emission shown in the lower or inverted "V" portion. The widths throughout the various portions of the "V" 's correspond to the associated timing uncertainties. The time scale for these illustrations is given by the arrow in the lower right-hand corner indicating a duration of 10 seconds. No representation of relative intensities has been attempted in this schematic.

2.3. Spectral and Temporal Parameters

Observed spectral and temporal parameters of the X-ray and microwave emission associated with the spike bursts are presented in Table 2. Following the event number is the time of maximum hard X-ray emission in Universal Time. The column labeled S_X gives a measure of the peak X-ray flux density, calculated according to the expression

$$S_X = \sum_{i=2}^{9} CH(i), \qquad (2)$$

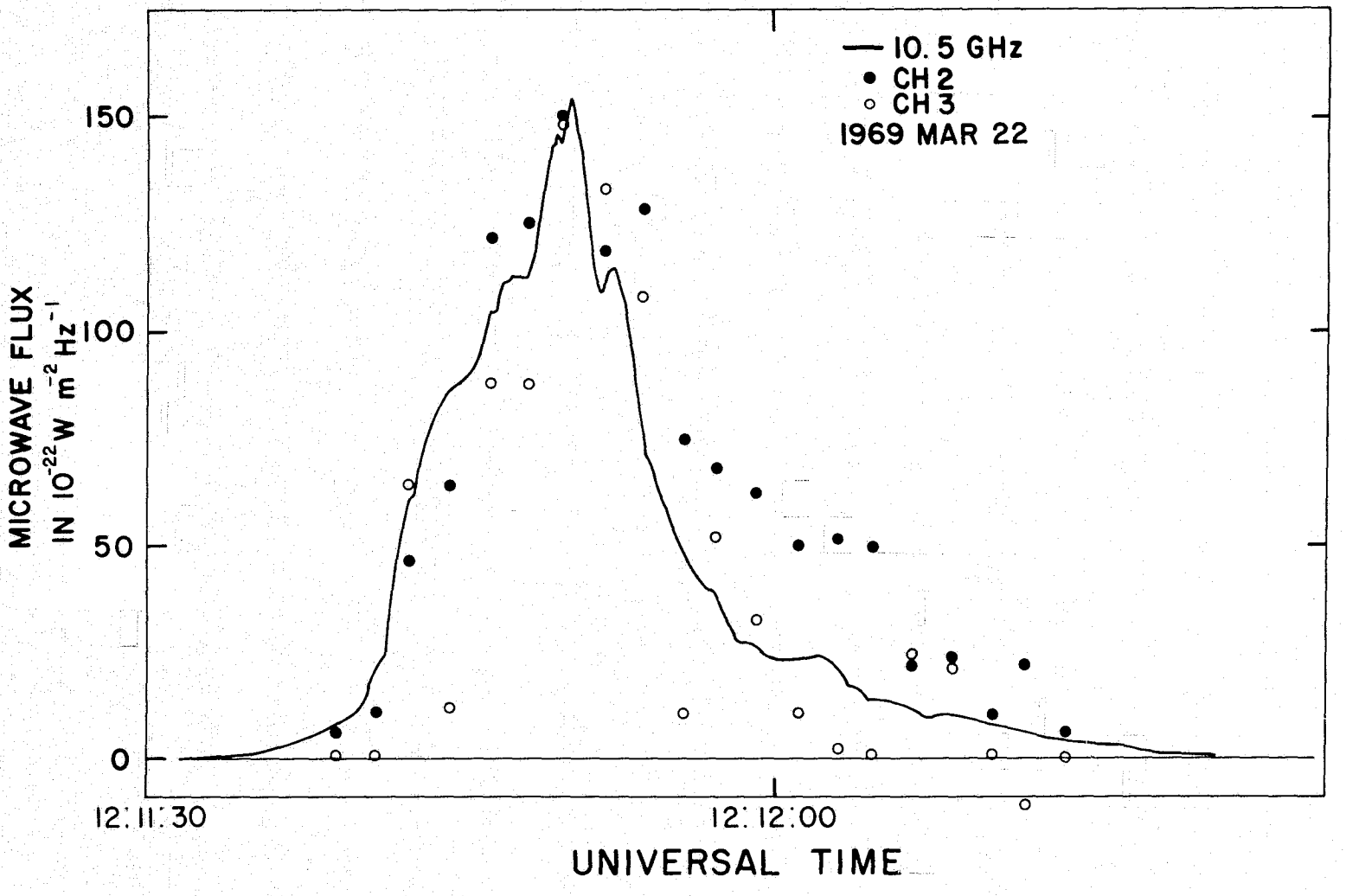

Figure 23. The time profiles of the X-ray flux in Channels 2 and 3 and the 10.5 GHz flux (Institute of Applied Physics, University of Bern), each normalized to the same peak height, for Event Number 5.

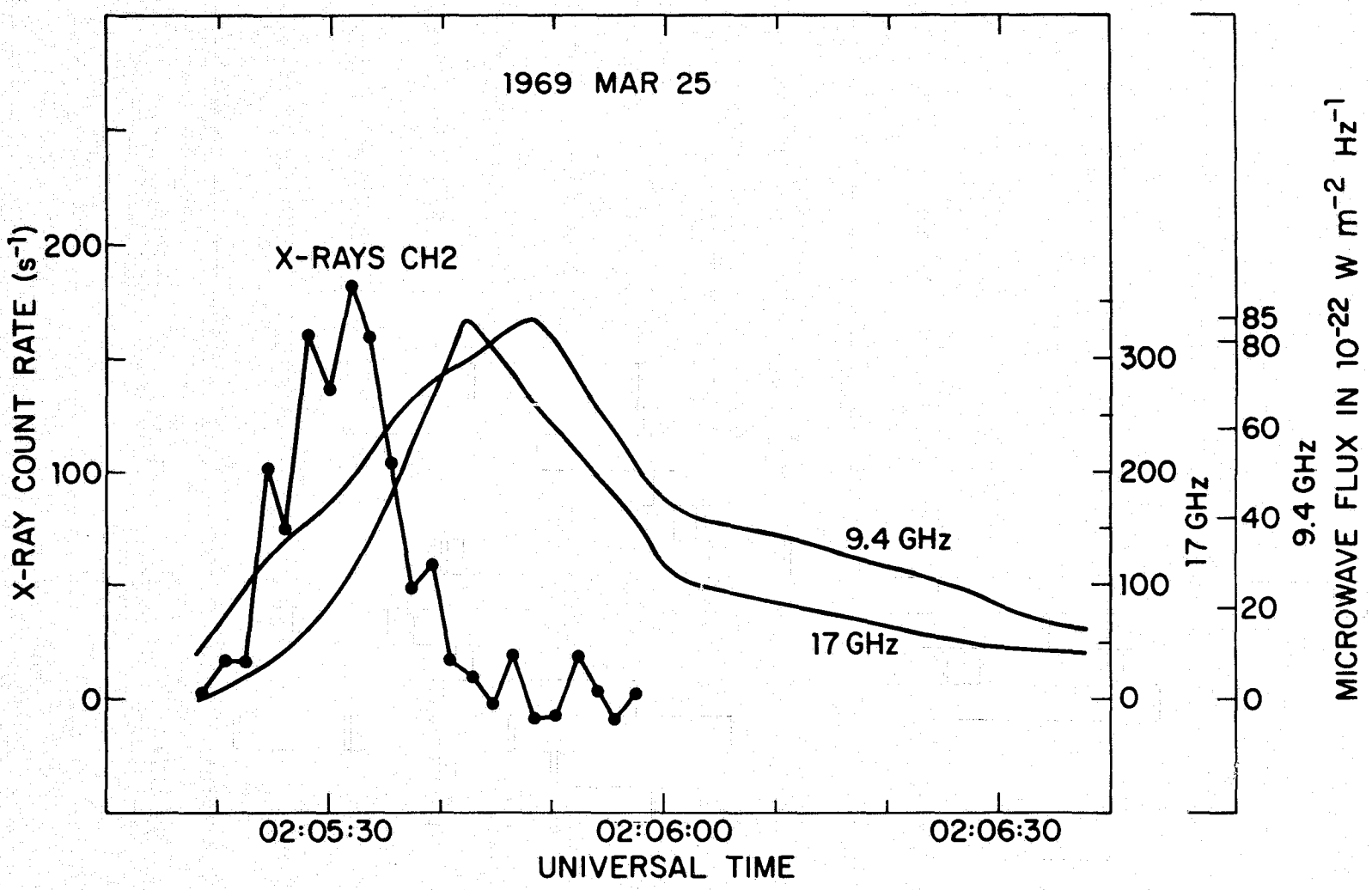

Figure 24. The time profiles of the X-ray flux in Channel 2, the 9.4 GHz flux (Institute of Atmospheric Research, Nagoya University, Toyokawa) and the 17 GHz flux (Solar Radio Section, Tokyo Astronomical Observatory) for Event Number 7.

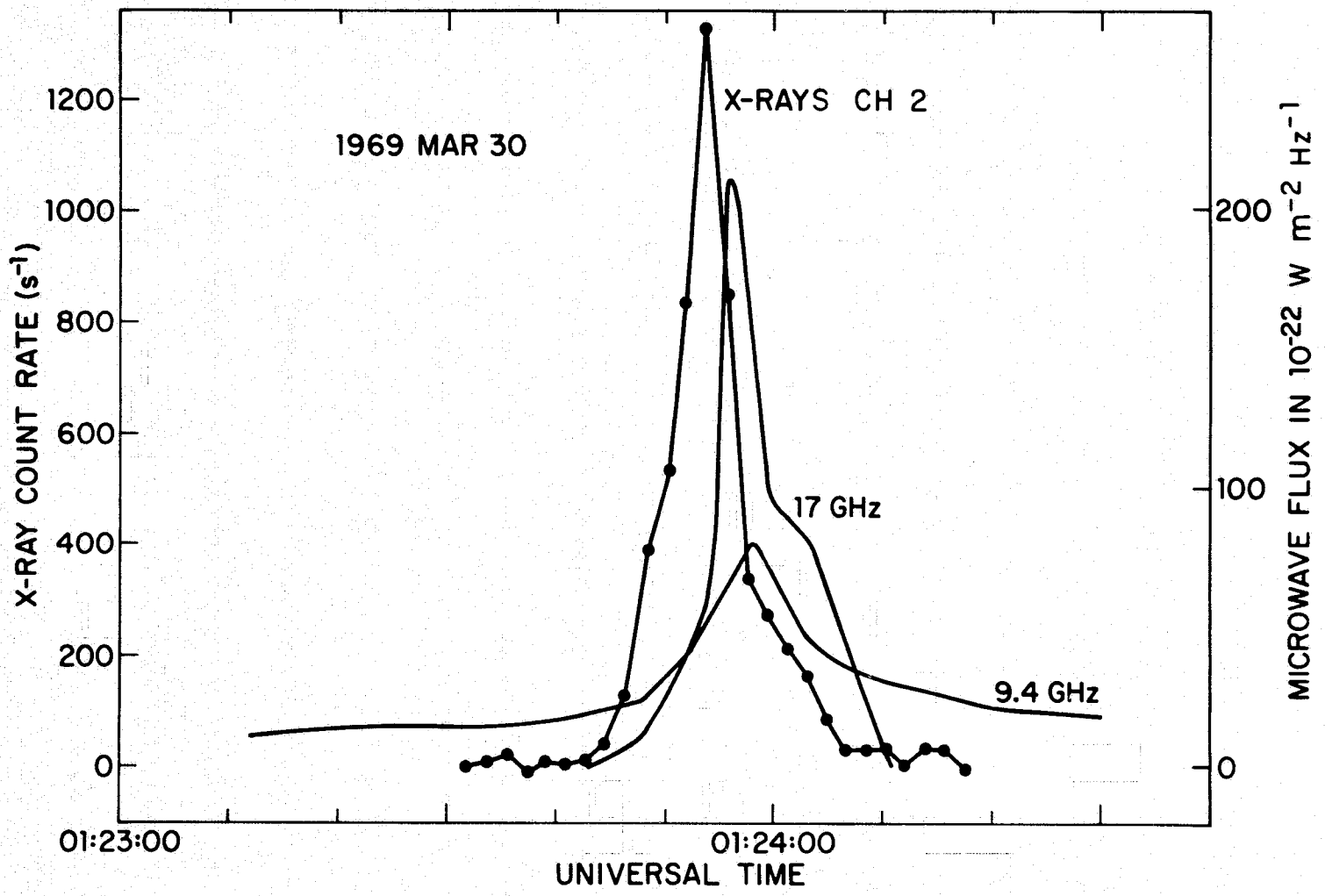

Figure 25. The time profiles of the X-ray flux in Channel 2, the 9.4 GHz flux (Institute of Atmospheric Research, Nagoya University, Toyokawa) and the 17 GHz flux (Solar Radio Section, Tokyo Astronomical Observatory) for Event Number 10.

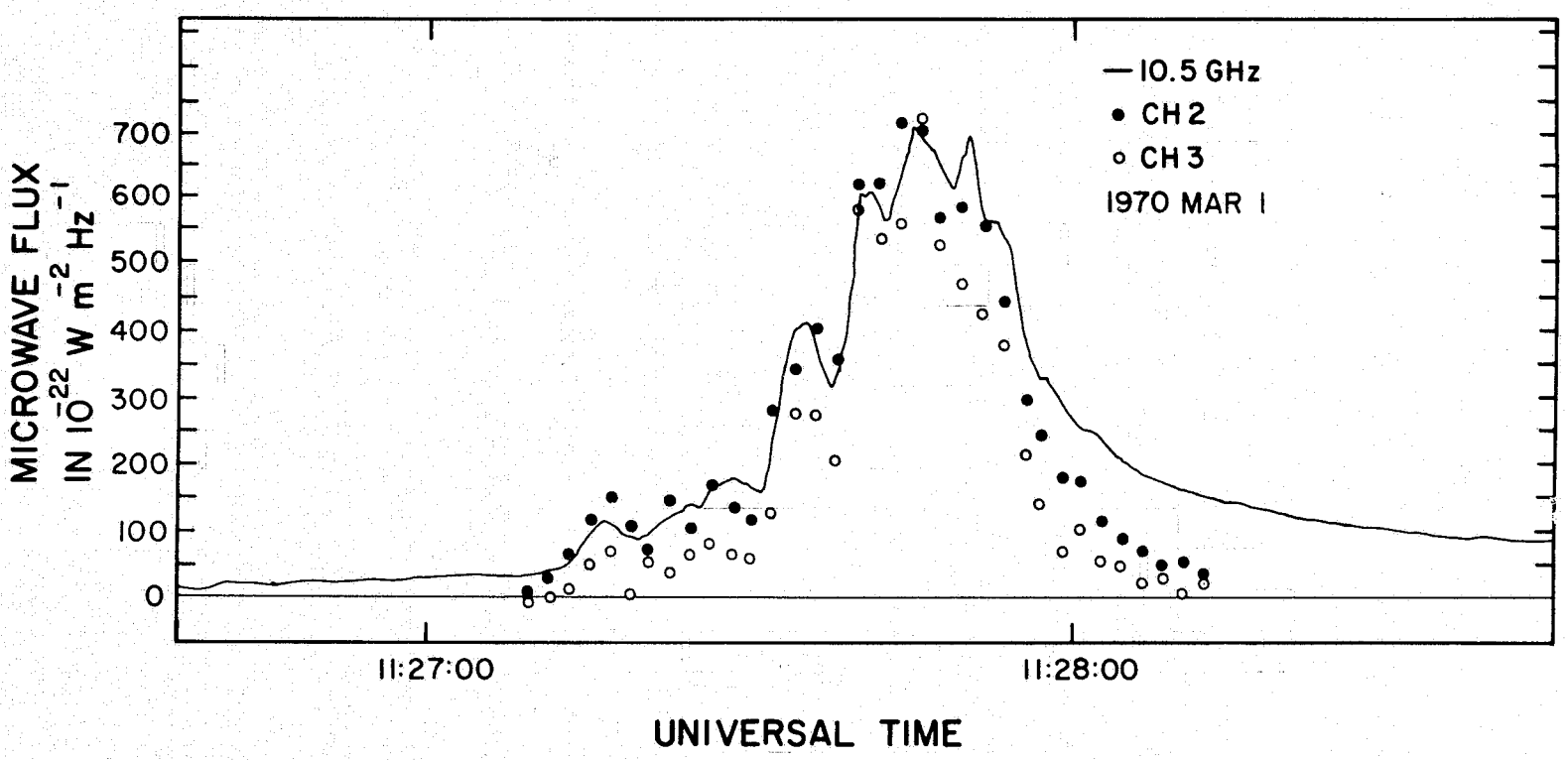

Figure 26. The time profiles of the X-ray flux in Channels 2 and 3 and the 10.5 GHz flux (Institute of Applied Physics, University of Bern) each normalized to the same peak height, for Event Number 12.

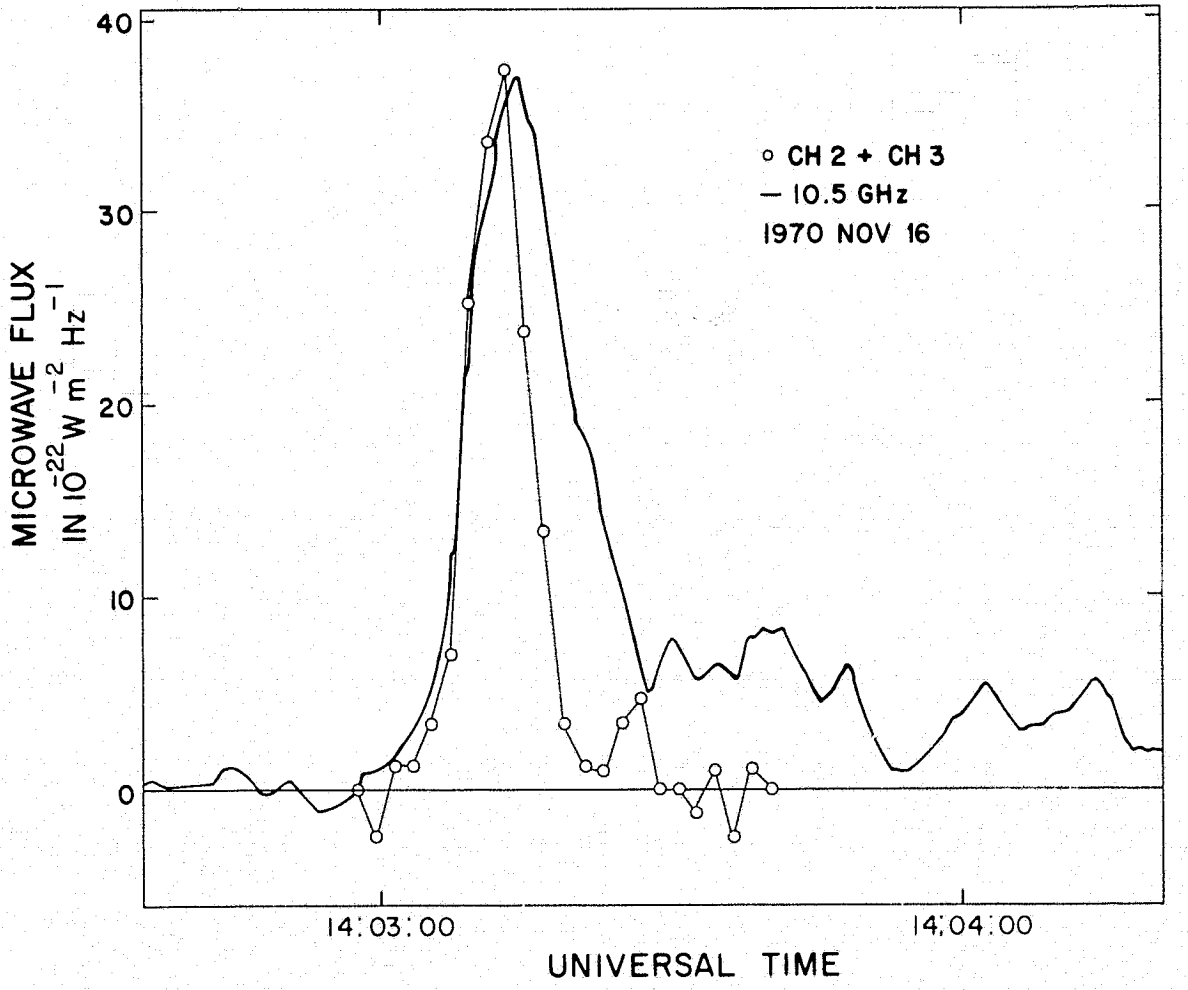

Figure 27. The time profiles of the sum of the X-ray flux in Channels 2 and 3 and the 10.5 GHz flux (Institute of Applied Physics, University of Bern) normalized to the same peak height for Event Number 19.

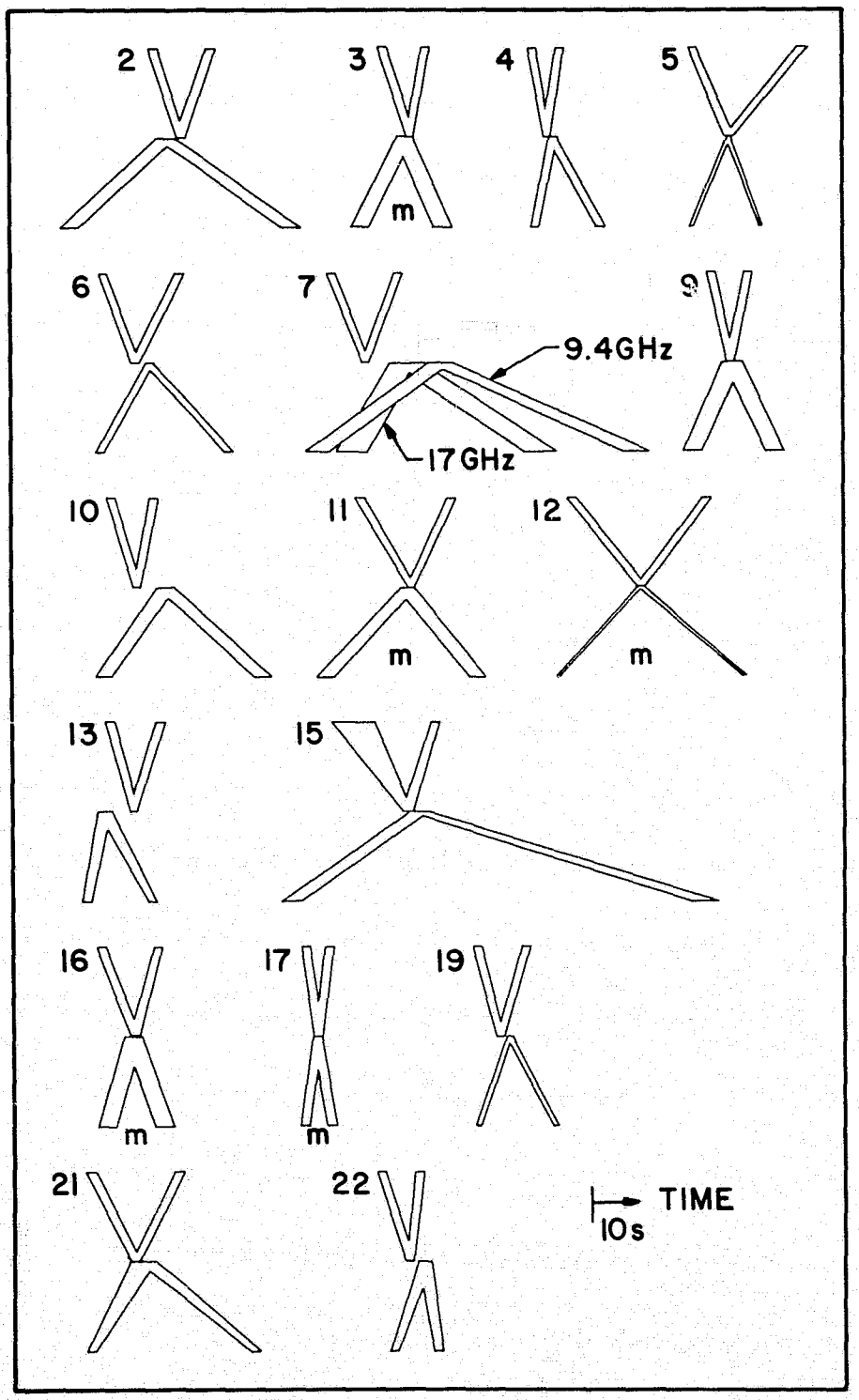

Figure 28. Schematic representation of the X-ray and microwave time profiles.

Table 2

Observed X-Ray and Microwave Parameters

N	X-Ray Peak Time						S_x	CH2	CH3	t_{xr}	t_x	S_μ	f_μ	S_2	f_2	$t_{\mu r}$	t_μ
	y	m	d	h	m	s	in Photons $cm^{-2}\ s^{-1}\ keV^{-1}$			in Seconds		in SFU	in GHz	in SFU	in GHz	in Seconds	
1	1969	3	1	6	6	41.5	0.29	0.27 ± 0.04	0.024 ± 0.012	6.0	11.5	46	8.80	22	5.0	—	—
2	1969	3	1	22	53	15.1	2.93	2.42 ± 0.15	0.440 ± 0.051	6.0	12.4	95	9.40	17	3.7	21.0	48.0
3	1969	3	8	22	7	7.1	0.21	0.18 ± 0.04	0.033 ± 0.015	5.9	9.5	20	3.75	15	3.5	10.0	18.0
4	1969	3	18	11	55	46.4	0.20	0.17 ± 0.04	0.021 ± 0.012	3.0	6.0	21	5.00	—	—	4.0	14.0
5	1969	3	22	12	11	49.9	0.33	0.25 ± 0.04	0.065 ± 0.018	8.0	24.0	150	10.50	84	5.0	8.4	15.1
6	1969	3	23	19	24	15.5	0.42	0.37 ± 0.03	0.045 ± 0.009	7.0	16.5	135	8.80	110	8.0	11.0	28.0
7	1969	3	25	2	5	31.9	0.27	0.22 ± 0.04	0.029 ± 0.013	7.4	15.0	335	17.00	145	11.0	21.0	66.0
8	1969	3	28	8	25	29.4	0.17	0.15 ± 0.03	0.016 ± 0.011	4.7	7.1	—	—	—	—	—	—
9	1969	3	29	7	37	45.9	0.20	0.17 ± 0.03	0.018 ± 0.008	4.1	8.2	15	9.50	—	—	9.0	18.0
10	1969	3	30	1	23	53.7	1.96	1.58 ± 0.12	0.250 ± 0.040	5.6	9.4	211	17.00	80	9.4	14.0	35.0
11	1969	7	7	5	38	12.8	1.27	1.04 ± 0.09	0.180 ± 0.030	11.3	20.3	655	2.00	—	—	18.0	33.0
12	1970	3	1	11	27	44.8	3.16	2.20 ± 0.10	0.650 ± 0.040	15.0	30.0	900	7.00	400	2.7	18.0	40.6
13	1970	6	14	12	50	51.9	0.44	0.32 ± 0.05	0.098 ± 0.022	4.4	10.4	52	15.40	52	15.4	4.0	14.0
14	1970	6	15	1	29	27.1	0.26	0.19 ± 0.04	0.058 ± 0.017	2.0	8.0	—	—	—	—	—	—
15	1970	6	15	18	38	18.2	0.34	0.31 ± 0.05	0.027 ± 0.013	12.0	19.0	200	8.80	77	3.0	29.0	92.0
16	1970	7	6	1	37	35.4	0.20	0.18 ± 0.04	0.017 ± 0.010	7.0	12.0	15	9.40	5	5.0	6.0	12.0
17	1970	8	12	21	7	55.8	0.51	0.39 ± 0.06	0.092 ± 0.021	2.4	4.8	64	15.40	24	10.0	3.0	7.0
18	1970	10	26	4	27	6.7	0.54	0.41 ± 0.04	0.093 ± 0.013	25.0	49.0	390	9.40	46	2.0	—	—
19	1970	11	16	14	3	11.7	0.20	0.17 ± 0.03	0.033 ± 0.010	4.8	10.8	40	10.00	—	—	7.3	18.5
20	1970	11	18	3	13	56.0	0.18	0.15 ± 0.03	0.021 ± 0.011	8.0	16.0	18	2.00	6	1.0	—	—
21	1971	4	19	18	31	4.4	0.16	0.15 ± 0.03	0.012 ± 0.009	9.5	19.1	117	15.40	75	8.8	12.0	36.0
22	1971	8	25	16	28	20.5	0.31	0.22 ± 0.04	0.062 ± 0.018	6.0	8.1	19	8.80	7	5.0	7.0	9.5

where CH(i) is the X-ray flux density observed in the i^{th} channel at the time of maximum hard X-ray emission, given in units of photons cm^{-2} s^{-1} keV^{-1}. When the flux density observed is less than the one standard deviation statistical uncertainty in that value, CH(i) for that observation is set equal to zero. Since these eight channels, 2 through 9, span approximately equal energy intervals, $S_X/8$ is the X-ray flux density in units of photons cm^{-2} s^{-1} keV^{-1} in the energy range 28 to 254 keV. The counting rates observed in Channel 1 are not employed in the present analysis. The columns labeled CH2 and CH3 present the X-ray flux density together with the associated one standard deviation uncertainty for Channels 2 and 3, respectively. The rise time of the hard X-ray spike burst is indicated by the symbol t_{xr} and the duration by the symbol t_x. The rise time is determined from the 28 to 82 keV counting rate as the time between the peak time and the time at which the rate rose to 1/4 of its peak value. The fall time is the time between the peak time and the time at which the rate fell to 1/4 of its peak value. This fraction was chosen because it is the lowest value which is above the background noise level for all 22 events. This choice enables the events to be characterized by the longest possible elapsed time which can be determined accurately and consistently. The duration is simply the sum of the rise time plus the fall time. The uncertainties in the X-ray rise times, fall times, and durations are between 1.4 and 2 seconds, due primarily to the instrumental sampling period.

The peak microwave flux density, labeled S_μ, was determined from the observations at the frequency $f_{\mu s}$ at which the greatest peak flux was observed. Because the microwave spectrum of many of these events is very steep and increases even at the highest observed frequency, the value given for S_μ is not, in many instances, the actual peak of the microwave emission. The microwave flux density S_2 is that observed at frequency f_2, the highest frequency at which the observed spectrum approximates the Rayleigh-Jeans Law, that is, the flux density is proportional to the square of the frequency. The flux densities are given in solar flux units (SFU) which is equivalent to 10^{-22} W m^{-2} Hz^{-1}. The uncertainties in the values of each of these parameters are due primarily to the lack of uniform, continuous spectral coverage at radio wavelengths. The rise time of the microwave emission in the frequency band nearest 10 GHz is indicated by the symbol $t_{\mu r}$, and the duration, by the symbol t_μ. The microwave rise times, fall times, and durations are determined in the same way as described for the corresponding X-ray parameters. The uncertainties in these parameters are between a fraction of a second and a few seconds.

2.4. Hα Observations

Characteristics of the Hα events closely associated in time with the hard X-ray spike bursts were obtained from the *Solar-Geophysical Data* records. The McMath plage region in which the Hα event was observed and the importance of

the event are presented in Table 3 in accord with standard *Solar-Geophysical Data* notation. Also given in Table 3 are the elapsed times between the peak of the hard X-ray spike burst and the Hα onset, the Hα peak, and the microwave peak. A negative value indicates that the hard X-ray peak preceded the other occurrence. The elapsed times with respect to Hα are given in minutes, where one minute is the resolution with which the Hα observations are reported. The elapsed times with respect to the microwave peak times are given in seconds, with uncertainties of 1 to 5 seconds. Histograms of the elapsed times are shown in Figures 19-31. Nonlinear times scales are employed in Figures 29 and 30 in order to simplify the presentation of the data.

2.5. Meterwave Observations

Dynamic spectra of the meterwave radiation observed in coincidence with two of the spike bursts are shown together with the time profiles of the hard X-ray emission in Figures 32 and 33. Event Number 12 occurred coincidently with strong meterwave emission which could be interpreted either as a type V burst or as a group of overlapping type III bursts. The event was preceded by a series of U bursts and followed by type II emission beginning approximately 100 seconds after the hard X-ray flare. Association of the meterwave emission with the hard X-ray spike burst is uncertain because two different regions were observed to be active in Hα on that day. One of these regions was seen to flare in Hα in coincidence with the hard X-ray burst, but the other was very active in association with type III radiation throughout the day (Urbarz, private communication). The most notable feature of Event Number 17 is its very short duration in hard X-rays which are simultaneous with decimetric radio emission. As can be seen in Figure 33, this radiation is the high frequency component of a reverse drift burst which is preceded by type III radiation and followed, after $\sim$200 seconds, by a type II burst.

Characteristics of the five meterwave bursts observed in coincidence with five of the hard X-ray spike bursts are summarized in Table 4. Question marks are used to indicate that the data records are not inconsistent with emission of the designated type, but that unambiguous identification is not possible. Meterwave coverage during the times of observation of the 22 X-ray spike bursts is complete except for Event Number 18 which occurred 1970 October 26 $04^h\ 27^m$ UT. The absence of reported meterwave bursts in coincidence with 16 of the spike bursts is, therefore, evidence that there was no meterwave emission associated with these events at or above the threshold levels of the Culgoora, Harvard, or Weissenau radio spectrographs.

Table 3

Observed Hα and Microwave Parameters

N	McMath Plage Region	Importance	Elapsed Time* Between X-Ray Peak and		
			Hα Onset	Hα Peak	Microwave Peak
			In Minutes		In Seconds
1	—	—	—	—	-6.5 ± 5.0
2	9957	-N	-0.7	-1.7	3.1 ± 2.5
3	9966	--B	1.1	-0.9	1.1 ± 2.5
4	9994	-B	1.8	-1.2	-1.6 ± 2.0
5	9994	--N	0.8	-2.2	-0.1 ± 1.0
6	9994 10001	-N -N	2.3 0.3	-1.7 -5.7	-3.5 ± 1.5
7	9994	-F	0.5	-1.5	-10.1 ± 3.0
8	9994	-F	0.5	-2.5	—
9	10014 10014	-N -N**	12.8 15.8	2.8 -30.2	-0.9 ± 2.5
10	10014	-N	1.9	-1.1	-6.3 ± 2.5
11	10181	1B	1.2	-0.8	0.8 ± 2.5
12	10595	2B**	0.7	-2.3	-0.2 ± 1.0
13	10789	1N**	28.9	-14.1	5.9 ± 2.5
14	10789	-B	-1.5	-18.5	—
15	10789	-B	1.3	-2.7	-2.8 ± 2.5
16	10808	-F	0.6	-2.4	-0.6 ± 2.5
17	10868	--N	1.9	-1.1	-0.2 ± 1.5
18	11002	1N**	16.1	-0.9	-5.3 ± 5.0
19	11029	-N	0.2	-0.8	-2.3 ± 1.0
20	—	—	—	—	-4.0 ± 5.0
21	11256	--N	1.1	-0.9	-2.6 ± 3.0
22	11482	--F	0.3	-1.7	-3.5 ± 2.0

*A minus sign indicates that the X-ray peak occurred prior to the designated emission.
**Unconfirmed flares reported in Solar-Geophysical Data.

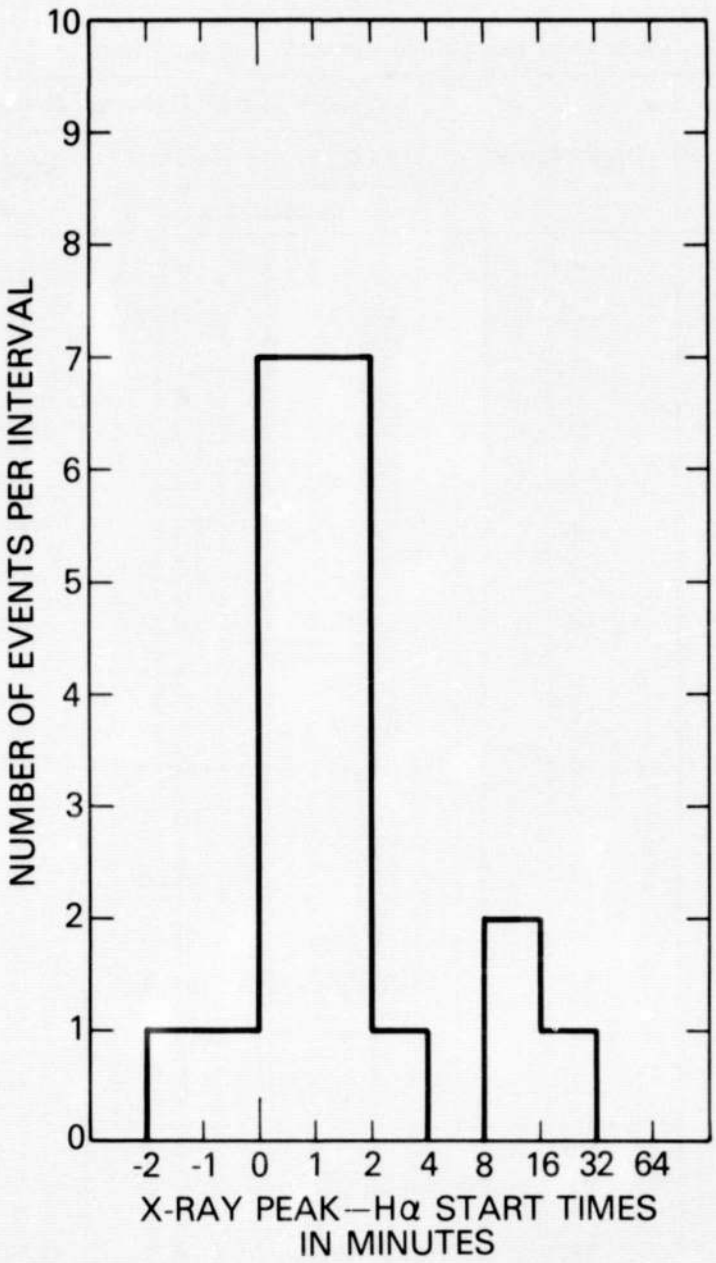

Figure 29. Histogram of elapsed times between the X-ray peak emission and the observed onset of the Hα emission. A negative value indicates that the X-ray peak occurred prior to the Hα onset. The time scale on the abcissa is nonlinear.

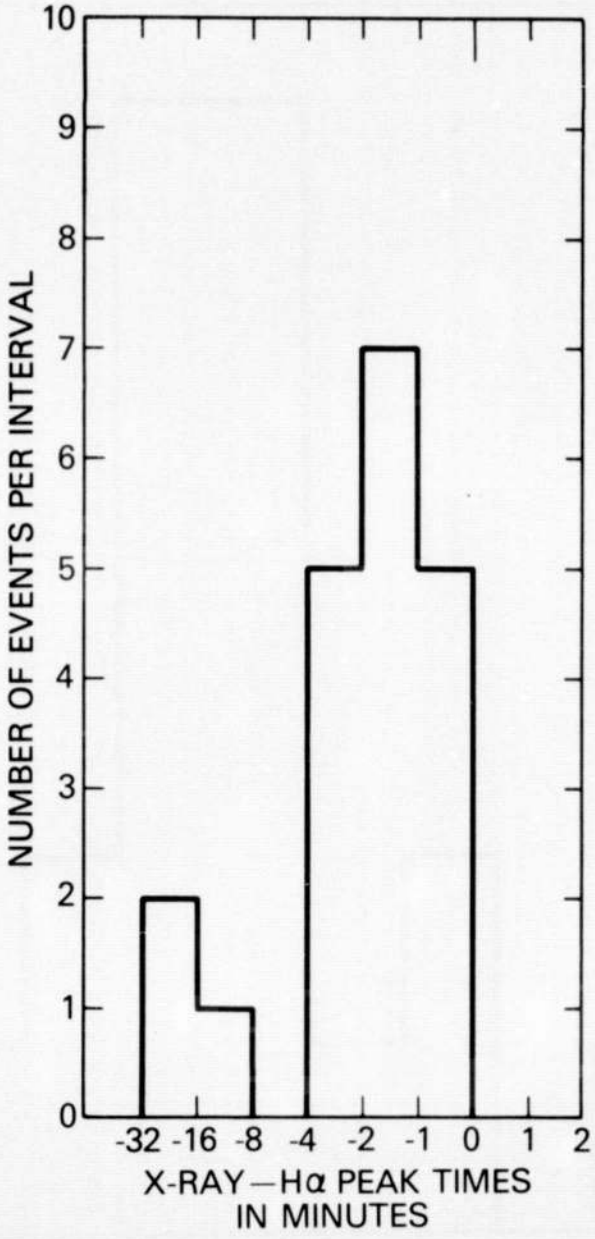

Figure 30. Histogram of elapsed times between the X-ray peak emission and the Hα maximum. A negative value indicates that the X-ray peak occurred prior to the maximum in the Hα emission. The time scale on abcissa is nonlinear.

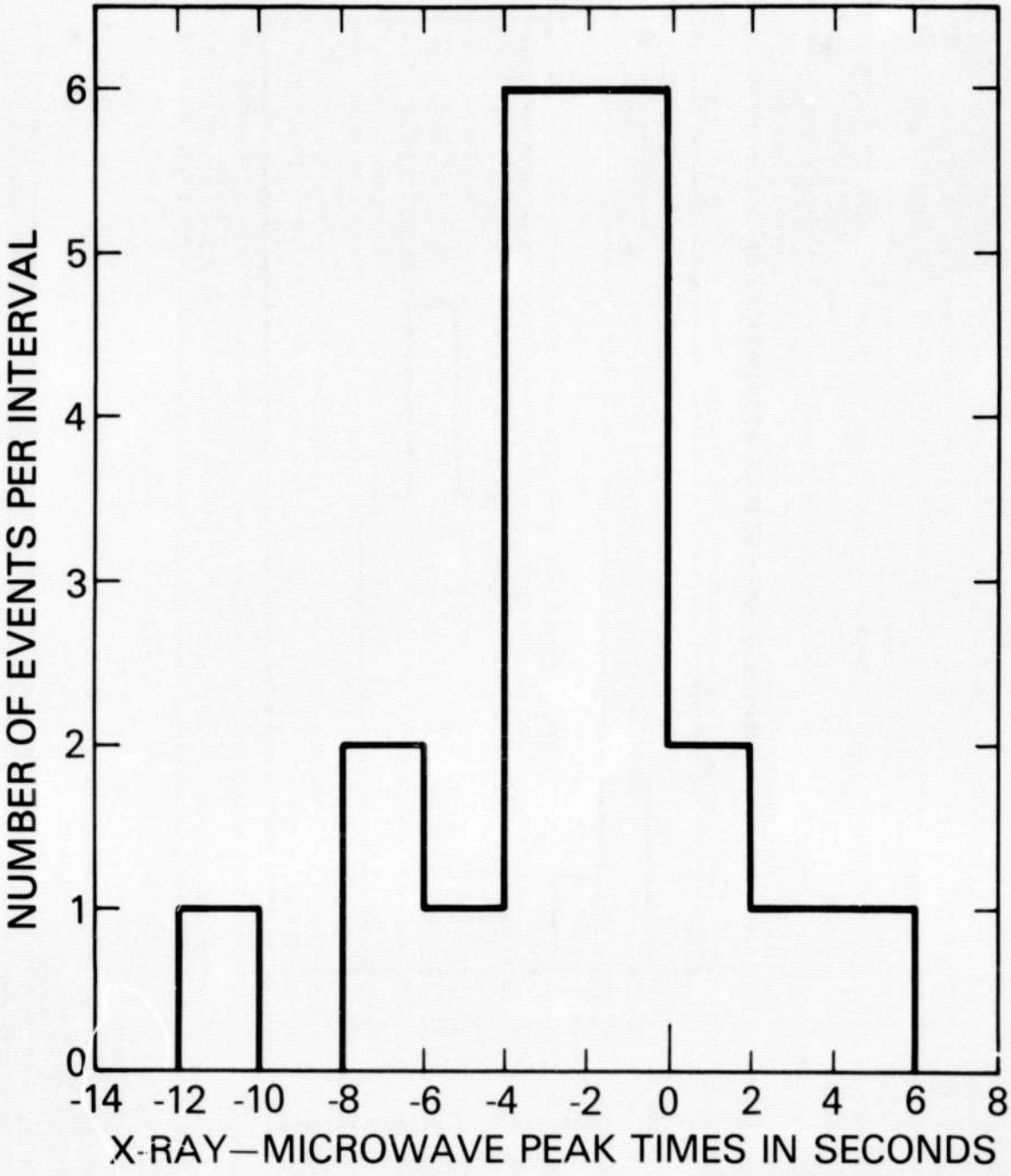

Figure 31. Histogram of elapsed times between X-ray peak emission and the microwave peak emission. A negative value indicates that the X-ray peak occurred prior to the maximum in the microwave.

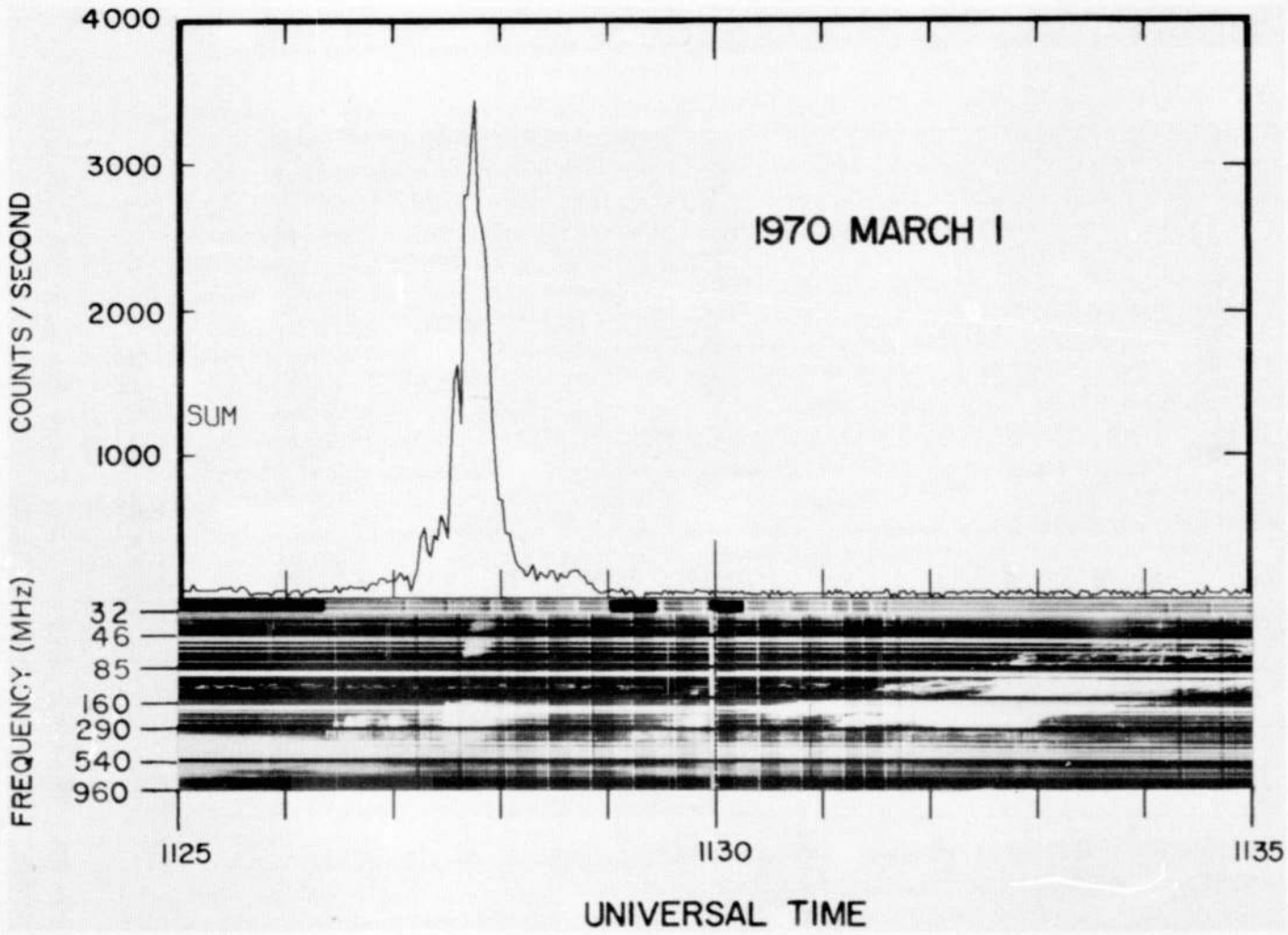

Figure 32. The time profiles of the X-ray flux summed over all the energy channels together with the dynamic meterwave spectrum (Astronomical Institute of the University of Tübingen, Weissenau) for Event Number 12.

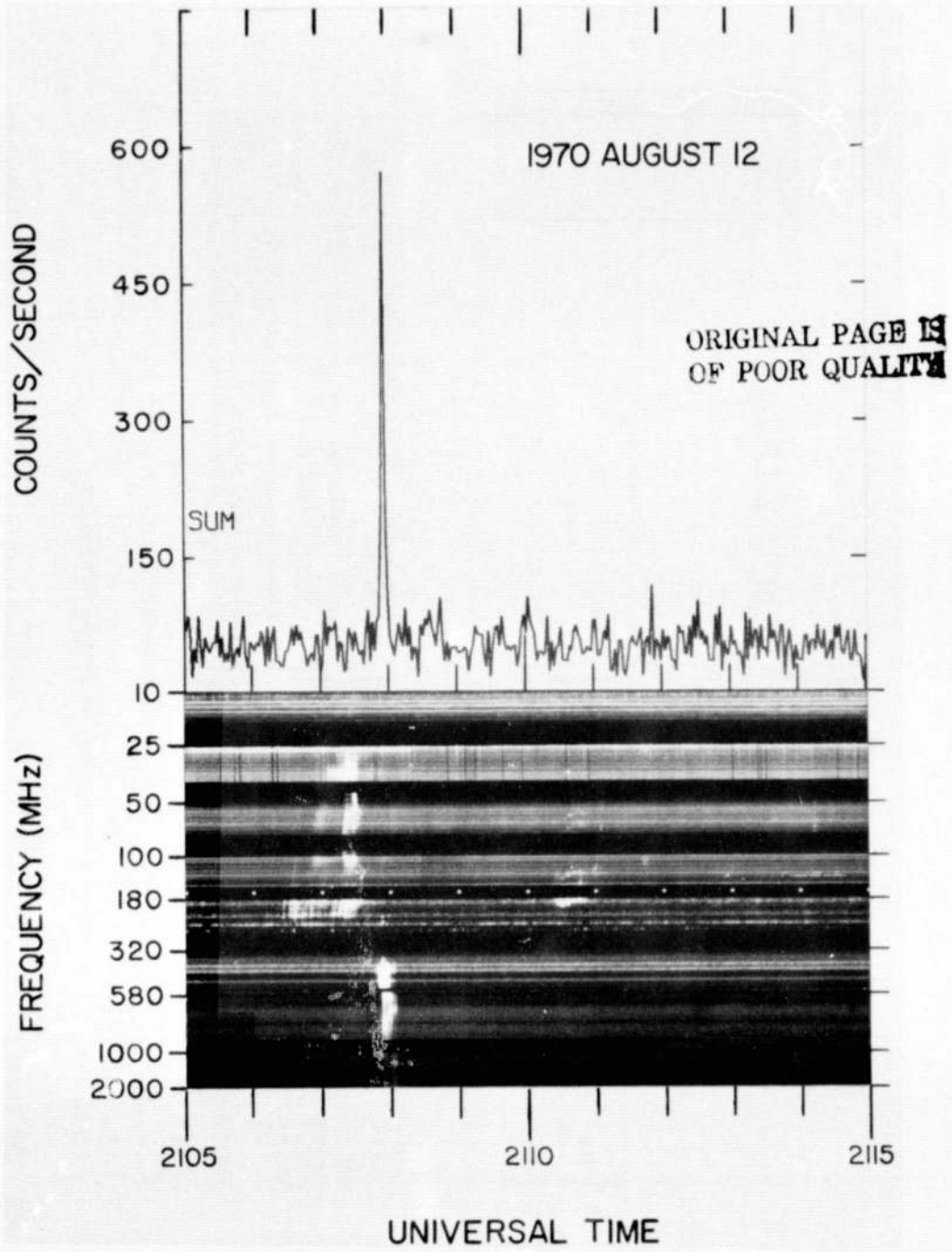

Figure 33. The time profiles of the X-ray flux summed over all the energy channels together with the dynamic meterwave spectrum (Harvard Radio Astronomy Station, Fort Davis) for Event Number 17.

Table 4

Meterwave Burst Types

N	II	III	V	U
3	no	no	yes	yes
11	yes	no	yes	yes
12	yes	?	?	yes
16	no	yes	yes	yes
17	yes	yes	?	?

3. DERIVED PARAMETERS

Physical parameters have been derived from the observational data to characterize the emitting regions and the energizing mechanisms associated with these impulsive flares. Calculations of such parameters are necessarily dependent on the emission models assumed. The numerical values of the derived parameters are expected to be most severely affected by the model dependence and should be considered as order of magnitude estimates only. On the other hand, the relative values of the parameters are less model dependent because all the calculations are based on the same, self-consistent physical assumptions. The correlations and relationships found between the various parameters are, therefore, considered to be of primary physical significance. The analysis reported in this section was found to be the simplest which yields reasonably self-consistent results for all the associated observations.

3.1. Geometry-Independent Parameters

The temperature of the emitting region has been calculated under the assumption that the X-rays are produced by bremsstrahlung radiation in an optically-thin thermal plasma. Backscattering of the X-rays from the solar photosphere has not been taken into account. According to Tucker (1975), the differential X-ray flux is related to the temperature and emission measure of the source as indicated in Equation (3),

$$I(E) = 1.07 \cdot 10^{3} \frac{\sum_i EM_i Z_i^2}{E \sqrt{T}} g_{ff}(E,T)\, e^{-E/T}, \qquad (3)$$

where I(E) is the differential X-ray flux in units of photons cm^{-2} s^{-1} keV^{-1} at a distance of 150×10^6 km from the emitting region; the energy, E, and the temperature, T, are in units of keV; EM_i is the emission measure of the ionic species with charge number Z_i in units of 10^{45} cm^{-3}; and g_{ff} (E, T) is the Gaunt factor. The emission measure is defined by the expression, $EM_i = n_e n_i V$; where n_e is the density of electrons; n_i is the density of ions with charge number Z_i; and V is the volume of the emitting region. From conservation of charge, $n_e = \sum_i n_i Z_i$. The sum, $\sum_i n_i Z_i^2$, is approximately equal to $1.2 n_e$ in a highly ionized plasma of solar composition so that $\sum_i EM_i Z_i^2$ in Equation (3) may be replaced by 1.2 EM, where $EM = n_e^2 V$. Tucker gives the following approximate expression for the Gaunt factor:

$$g_{ff}(E,T) \approx \left(\frac{T}{E}\right)^{0.4}, \text{ for } T \lesssim E. \qquad (4)$$

With the foregoing simplifications, Equation (3) may be written as

$$I(E) = 1.3 \cdot 10^3 \frac{EM\, e^{-E/T}}{E^{1.4}\, T^{0.1}} . \qquad (5)$$

The relationship given in Equation (5) was employed to calculate the temperature and emission measure at the time of peak flux for each of the impulsive spike bursts.

The temperatures calculated from the peak X-ray flux densities observed in Channel 2 and in Channel 3, together with the associated statistical uncertainties, are presented in Table 5 in the column labeled $T_{CH2/CH3}$. The symbol N_T designates the number of channels, including Channel 2, which show a statistically significant flux above background. The mean temperature at the time of peak flux is the average of the individual values determined from the ratio of the flux density in Channel 2 to the statistically significant flux densities in the higher channels. That is

$$T = \frac{1}{N_T - 1} \sum_{i=3}^{N_T+1} T_{CH2/CHi} . \qquad (6)$$

The uncertainties in each of the individual temperatures, $T_{CH2/CHi}$, were found to be approximately equal to the uncertainty in $T_{CH2/CH3}$ for the same event, with the greater statistical uncertainties in the higher channels being compensated by the greater difference in energies. Only two events, Numbers 7 and 10, show significant deviations from a single temperature characterizing the X-ray spectrum at the peak of the burst.

Also presented in Table 5 is the emission measure, EM, calculated according to Equation (5) with I(E) set equal to the X-ray flux density in Channel 2 and T set equal to the mean temperature as defined by Equation (6).

The classical expression for low-frequency radiation from a homogeneous thermal plasma is given in Equation (7). (See, for example, Zheleznyakov 1970, Chapter 22.)

$$S(f) = 0.16\, f^2\, A_\mu\, T \left(1 - \frac{e^{-\tau_o(f)} + e^{-\tau_e(f)}}{2}\right), \qquad (7)$$

where S(f) is the microwave flux density at a distance of 150×10^6 km from the source in units of 10^{-22} $W m^{-2}$ Hz^{-1} at frequency f, in GHz; A_μ is the projected

Table 5

Geometry-Independent Derived Parameters

N	N_T	$T_{CH2/CH3}$ in keV	T in keV	EM in 10^{45} cm^{-3}	A_μ in 10^{18} cm^2	A_α in 10^{18} cm^2
1	2	16 ± 5	16	0.48	0.34	—
2	4	28 ± 4	24	2.15	0.33	2.24
3	2	29 ± 19	29	0.12	0.27	0.72
4	3	20 ± 11	28	0.12	—	2.67
5	3	45 ± 33	39	0.12	0.55	1.11
6	3	20 ± 3	19	0.45	0.56	1.09
7	3	21 ± 9	42	0.10	0.18	0.91
8	2	18 ± 10	18	0.21	—	0.60
9	3	18 ± 6	26	0.13	—	1.33
10	4	25 ± 4	32	0.95	0.18	1.11
11	3	27 ± 5	29	0.70	—	4.50
12	5	58 ± 10	52	0.88	6.65	6.34
13	3	63 ± 57	54	0.12	0.03	4.69
14	3	62 ± 92	46	0.08	—	2.79
15	2	16 ± 5	16	0.57	3.37	0.25
16	2	17 ± 7	17	0.30	0.08	0.99
17	3	39 ± 18	42	0.18	0.04	0.66
18	4	37 ± 9	36	0.22	2.03	4.54
19	2	30 ± 14	30	0.11	—	0.78
20	3	22 ± 12	34	0.08	1.11	—
21	2	15 ± 7	15	0.31	0.40	0.75
22	3	52 ± 53	63	0.08	0.03	0.75

area in units of 10^{18} cm^2; and T is the temperature of the source in keV. The frequency-dependent optical depths of the ordinary and the extraordinary modes are $\tau_o(f)$ and $\tau_e(f)$, respectively. For temperatures above 1 keV and typical solar magnetic fields, the emission and absorption processes are dominated by gyrosynchrotron emission and self absorption (Drummond and Rosenbluth 1960 and 1963, Trubnikov 1961). The microwave emission is assumed to be gyrosynchrotron radiation from the same thermal electrons which produce the observed hard X-ray emission. Under these conditions, the plasma is optically thick up to high harmonics (20 to 30) of the gyrofrequency, in which case, Equation (7) reduces to the Rayleigh-Jeans approximation,

$$S(f) = 0.16\, f^2\, A_\mu\, T. \tag{8}$$

The applicability of this result was verified in the present work from calculations of the emission and absorption coefficients based on the analysis and the computer program developed by Ramaty (1969).

As defined in the previous section, $S(f_2)$ is S_2 and f_2 is the highest frequency for which the microwave spectrum was found to agree with the relationship given in Equation (8). Thus it follows that

$$A_\mu = \frac{6.3\, S_2}{T\, f_2^2}. \tag{9}$$

The values of A_μ, presented in Table 5, have been determined from the values of S_2, f_2, and T given in Tables 4 and 5. The measured areas of the associated Hα flares, reported in the *Solar-Geophysical Data* records, $A_{H\alpha}$, are also presented in Table 5.

3.2. Geometry-Dependent Parameters

In Table 6, the flare parameters which depend on the geometry of the emitting region are presented. The diameter, D, and the volume, V, are calculated under the assumption that the emitting region is approximately spherically symmetric. These parameters are obtained from A_μ according to the relationships

$$D = (A_\mu)^{1/2}, \tag{10}$$

where D is in units of 10^9 cm, and

$$V = (A_\mu)^{3/2}, \tag{11}$$

where V is in units of 10^{27} cm^3.

The density, in units of 10^9 cm^{-3}, is calculated according to the relationship

$$n_e = \left(\frac{EM}{V}\right)^{1/2}, \qquad (12)$$

Table 6

Geometry-Dependent Derived Parameters

N	D in 10^9 cm	V in 10^{27} cm^3	n_e in 10^9 cm^{-3}	ED in erg cm^{-3}	U in 10^{27} erg	t_c in s
1	0.59	0.200	1.60	120	24	10
2	0.58	0.190	3.40	380	73	8
3	0.52	0.140	0.94	130	18	41
5	0.74	0.410	0.55	100	42	110
6	0.75	0.420	1.00	98	41	20
7	0.43	0.080	1.20	230	18	58
10	0.42	0.080	3.50	540	41	13
12	2.58	17.200	0.23	56	970	410
13	0.16	0.004	5.50	1400	6	18
15	1.84	6.190	0.30	23	140	53
16	0.27	0.020	3.80	310	6	4
17	0.19	0.007	5.20	1000	7	13
18	1.42	2.890	0.28	47	140	190
20	1.05	1.160	0.27	44	51	190
21	0.63	0.250	1.10	81	20	14
22	0.16	0.004	4.20	1300	6	30

where n_e is, strictly speaking, the electron density, but also to a good approximation, the ion density as well. The energy density of the flare source at burst maximum is calculated with the assumption that the temperature and the density of the ions are the same as those of the electrons. For n_e in units of 10^9 cm^{-3} and T in units of keV, the energy density is given by

$$ED = 4.8\, n_e T, \tag{13}$$

where ED in units of erg cm^{-3}. The total energy, U, of the thermal plasma is given by

$$U = V \cdot ED, \tag{14}$$

where U is in units of 10^{27} erg.

The final parameter presented in Table 6 is t_c, the collision time defined by the expression

$$t_c = \frac{0.25\, T^{3/2}}{n_e}, \tag{15}$$

where t_c is in seconds. The collision time was derived from the energy exchange rate of an electron in a plasma as given by Tucker (1975) with the electron kinetic energy set equal to the mean thermal energy of the plasma. To within a constant factor of approximately 2, t_c is equal to the self-collision time defined by Spitzer (1962) as the time required for a monoenergetic distribution of particles to assume a Maxwellian distribution of the same mean energy. Again it should be noted that the absolute values of the derived parameters, especially those related to the flare geometry, are quite sensitive to details of the models assumed. Their primary significance, therefore, lies in their variations relative to the variations in other flare parameters.

Correlation coefficients between various pairs of observational and derived parameters have been calculated together with the probability, $P(r, \nu)$, that a random distribution with the same number of pairs would show a stronger correlation (Bevington 1969). In Table 7, $P(r, \nu)$ designates the probability; r, the correlation coefficients; and ν, the number of degrees of freedom which is 2 less than the number of pairs. All those pairs for which the probability is $\gtrsim 50\%$, implying that such a correlation is expected to occur by chance in $\gtrsim 50\%$ of random distributions, are listed as NOT CORRELATED. The parameter pairs are listed, within subsections, in order of increasing probability. For all those pairs for

Table 7

Parameter Correlations and Coefficients

Times						
x	y	P(r, ν)	r	ν	a	b
t_{xr}	t_{xf}	0.000017	0.85	20	-0.50	1.04
$t_{\mu r}$	$t_{\mu f}$	0.000062	0.89	15	-5.60	2.17
$t_{\mu r}$	t_{xr}	0.022	0.69	15	1.57	0.46
t_{xr}	$t_{\mu f}$	0.20	0.52	15	—	—
t_x	t_μ	0.38	0.44	15	—	—
$t_{\mu r}$	t_{xf}	Not Correlated		—	—	—
$t_{\mu f}$	t_{xf}	Not Correlated		—	—	—

Times and Intensities						
x	y	P(r, ν)	r	ν	a	b
(LOG(S_μ)	(LOG($S_x t_x$)	0.00022	0.82	18	-0.99	0.91
LOG($S_\mu t_\mu$)	LOG($S_x t_x$)	0.0027	0.79	15	-1.46	0.67
LOG(t_x)	LOG(S_μ)	0.012	0.68	18	-0.76	2.36
LOG(S_μ)	LOG(S_x)	0.021	0.65	18	-1.73	0.71
LOG(t_μ)	LOG(S_μ)	0.030	0.67	15	-0.60	1.85
LOG($t_{\mu f}$)	LOG(S_μ)	0.048	0.64	15	0.16	1.55
LOG($S_\mu t_\mu$)	LOG(S_x)	0.083	0.60	15	—	—
LOG(S_2)	LOG($S_x t_x$)	0.15	0.56	14	—	—

Table 7 (Continued)

x	y	P(r, ν)	r	ν	a	b
LOG($S_2\, t_\mu$)	LOG($S_x\, t_x$)	0.15	0.62	11	—	—
LOG(t_μ)	LOG($S_x\, t_x$)	0.16	0.54	15	—	—
LOG(CH3/CH2)	LOG(S_x/t_x)	0.20	0.46	20	—	—
LOG(CH3/CH2)	LOG(S_x)	0.36	0.40	20	—	—
LOG(S_2)	LOG(S_x)	Not Correlated		—	—	—
LOG(CH3/CH2)	LOG($S_x\, t_x$)	Not Correlated		—	—	—
LOG($S_2\, t_\mu$)	LOG(S_x)	Not Correlated		—	—	—
LOG(t_x)	LOG(S_x)	Not Correlated		—	—	—
LOG(CH3/CH2)	LOG(t_{xr})	Not Correlated		—	—	—
LOG($t_{\mu r}$)	LOG(S_μ)	Not Correlated		—	—	—

Times, Intensities, and Derived Parameters						
x	y	P(r, ν)	r	ν	a	b
LOG(t_x)	LOG(n)	0.0028	-0.81	14	2.47	-2.06
LOG(t_x)	LOG(D)	0.0034	0.80	14	-1.96	1.48
LOG(t_x)	LOG(ED)	0.0091	-0.76	14	4.91	-2.30
LOG(t_x)	LOG(t_c)	0.047	0.66	14	-1.16	2.32
LOG(t_x)	LOG(A_α)	Not Correlated		—	—	—
LOG(t_x)	LOG(T)	Not Correlated		—	—	—
LOG(f_2)	LOG(n)	0.025	0.70	14	-1.02	1.60

Table 7 (Continued)

x	y	P(r, ν)	r	ν	a	b
LOG(f_2)	LOG(D)	0.050	-0.65	14	0.56	-1.15
LOG(f_2)	LOG(ED)	0.053	0.65	14	1.00	1.79
LOG(f_2)	LOG(A_α)	Not Correlated		—	—	—
LOG(f_2)	LOG(T)	Not Correlated		—	—	—
LOG(U)	LOG(A_α)	Not Correlated		—	—	—
LOG(A_μ)	LOG(A_α)	Not Correlated		—	—	—

which the probability is $\lesssim 5\%$, a and b are given also to characterize the relationship between the parameters x and y,

$$y = a + bx. \tag{15}$$

To determine a and b, two unweighted, linear least-squares fits were performed; first determining parameters a_{xy} and b_{xy} by minimizing $\sum (y - a_{xy} - b_{xy}\, x)^2$ and then determining a_{yx} and b_{yx} by minimizing $\sum (x - a_{yx} - b_{yx}\, y)^2$. The geometrical mean of the two fits is obtained by defining

$$b = \sqrt{\frac{b_{xy}}{b_{yx}}}, \tag{16}$$

and

$$a = \frac{a_{xy} + b_{xy}\, a_{yx} - b(a_{yx} + b_{yx}\, a_{xy})}{1 - b_{xy}\, b_{yx}}. \tag{17}$$

The parameter pairs for which strong correlations have been found are shown in Figures 34-50. A correlation between X-ray rise time and X-ray spectral index was reported by Vorpahl and Takakura (1974), but was not found in the present work as can be seen in Figure 43. The significance of the parameters and correlations is discussed in the following section.

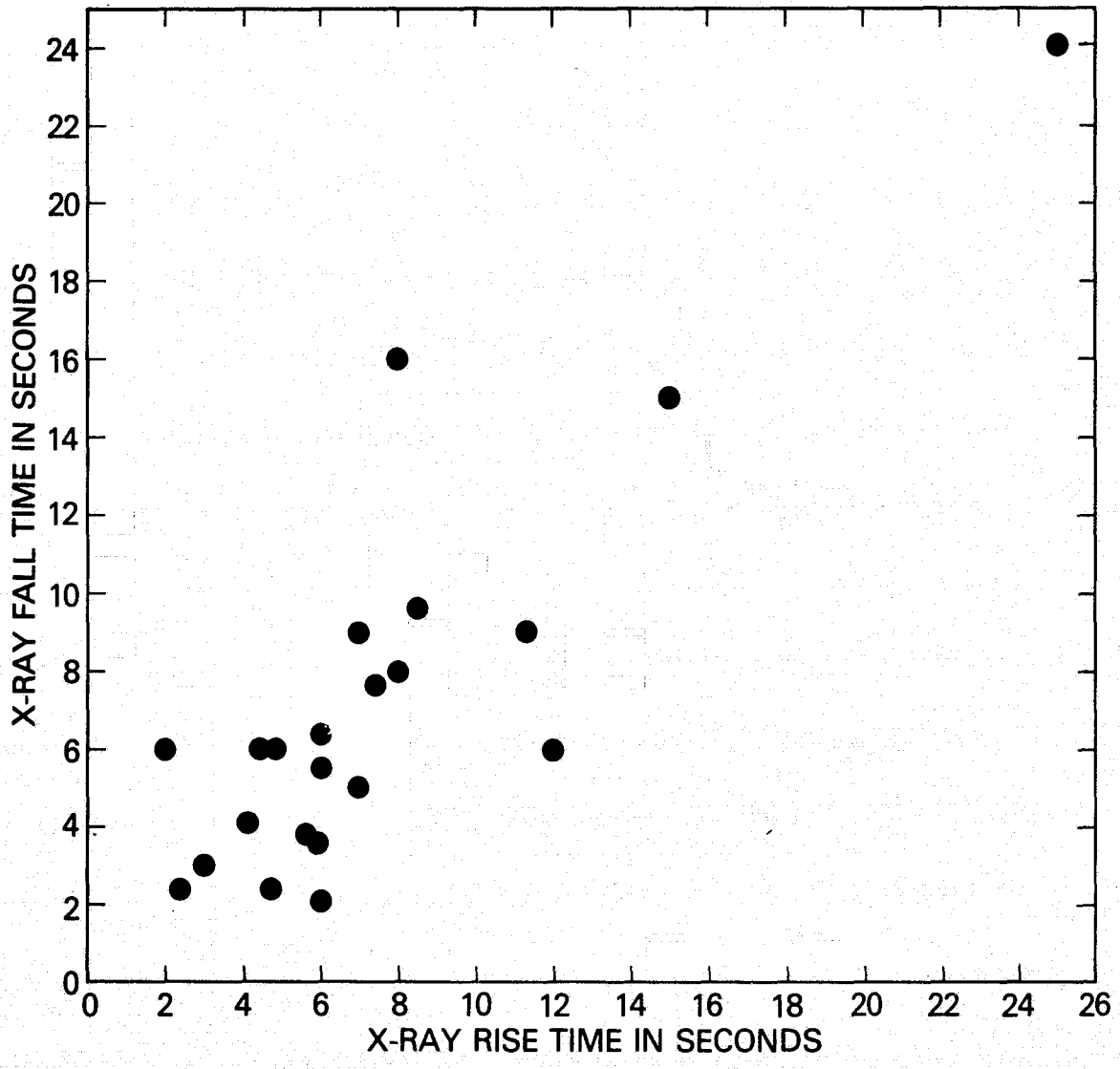

Figure 34. Scatter Plot of t_{xf} Versus t_{xr}.

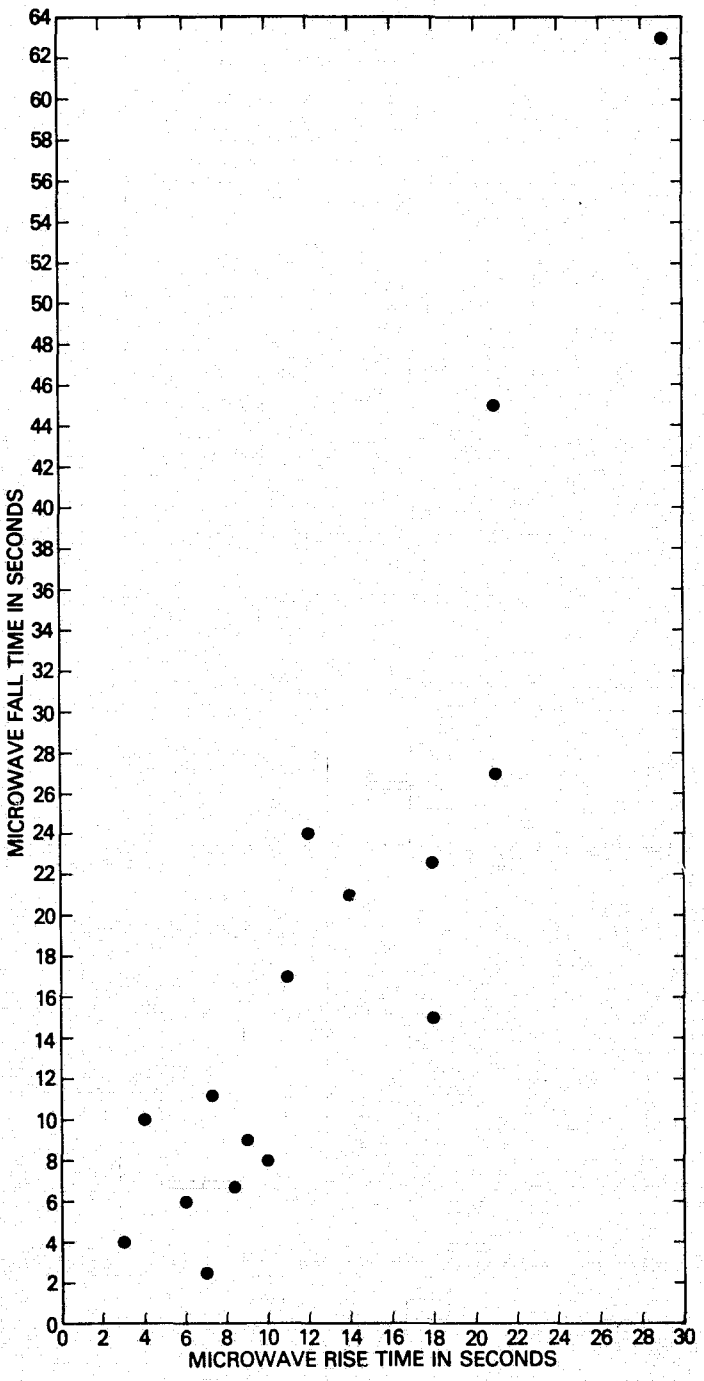

Figure 35. Scatter Plot of $t_{\mu f}$ Versus $t_{\mu r}$.

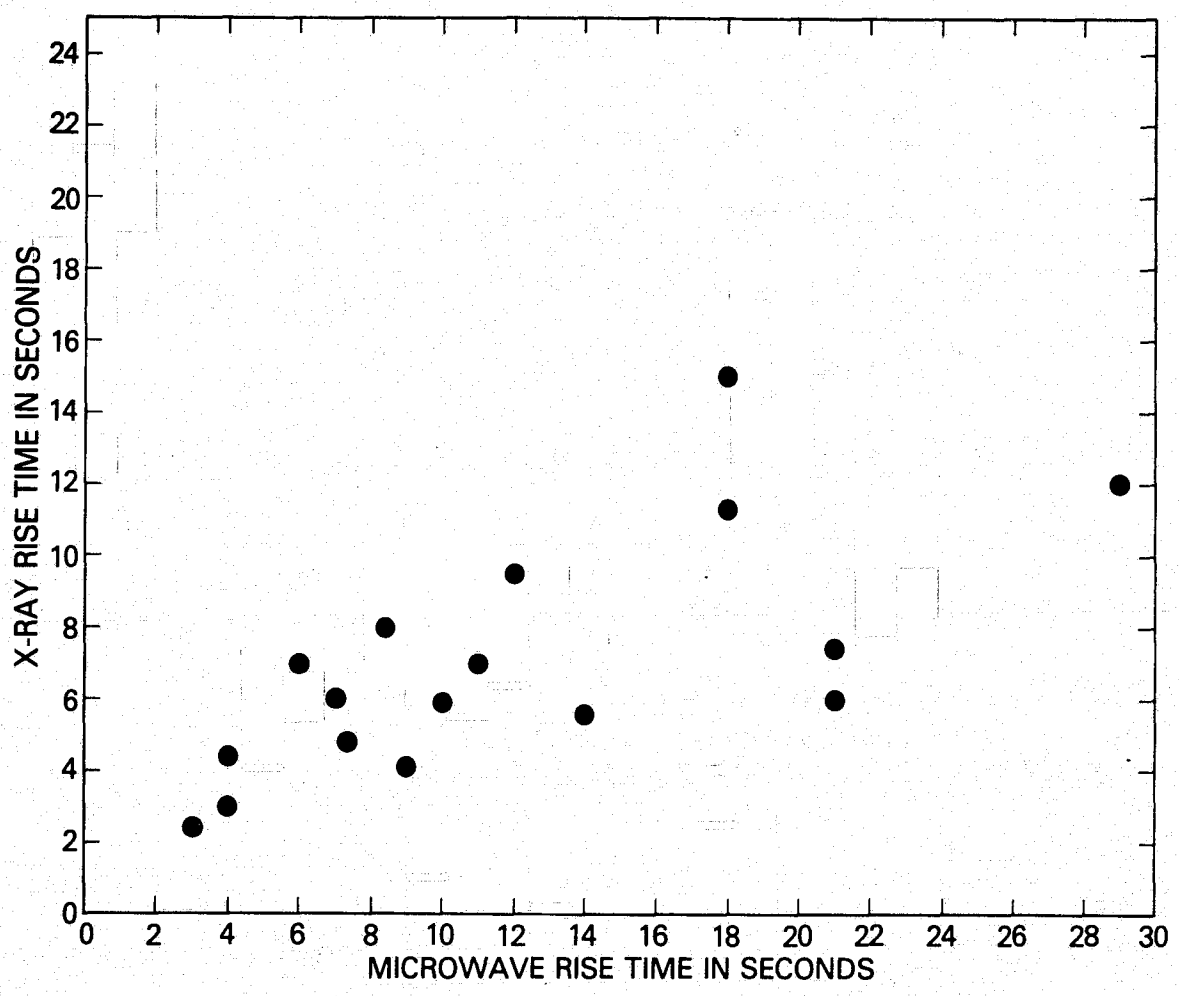

Figure 36. Scatter Plot of t_{xr} Versus $t_{\mu r}$.

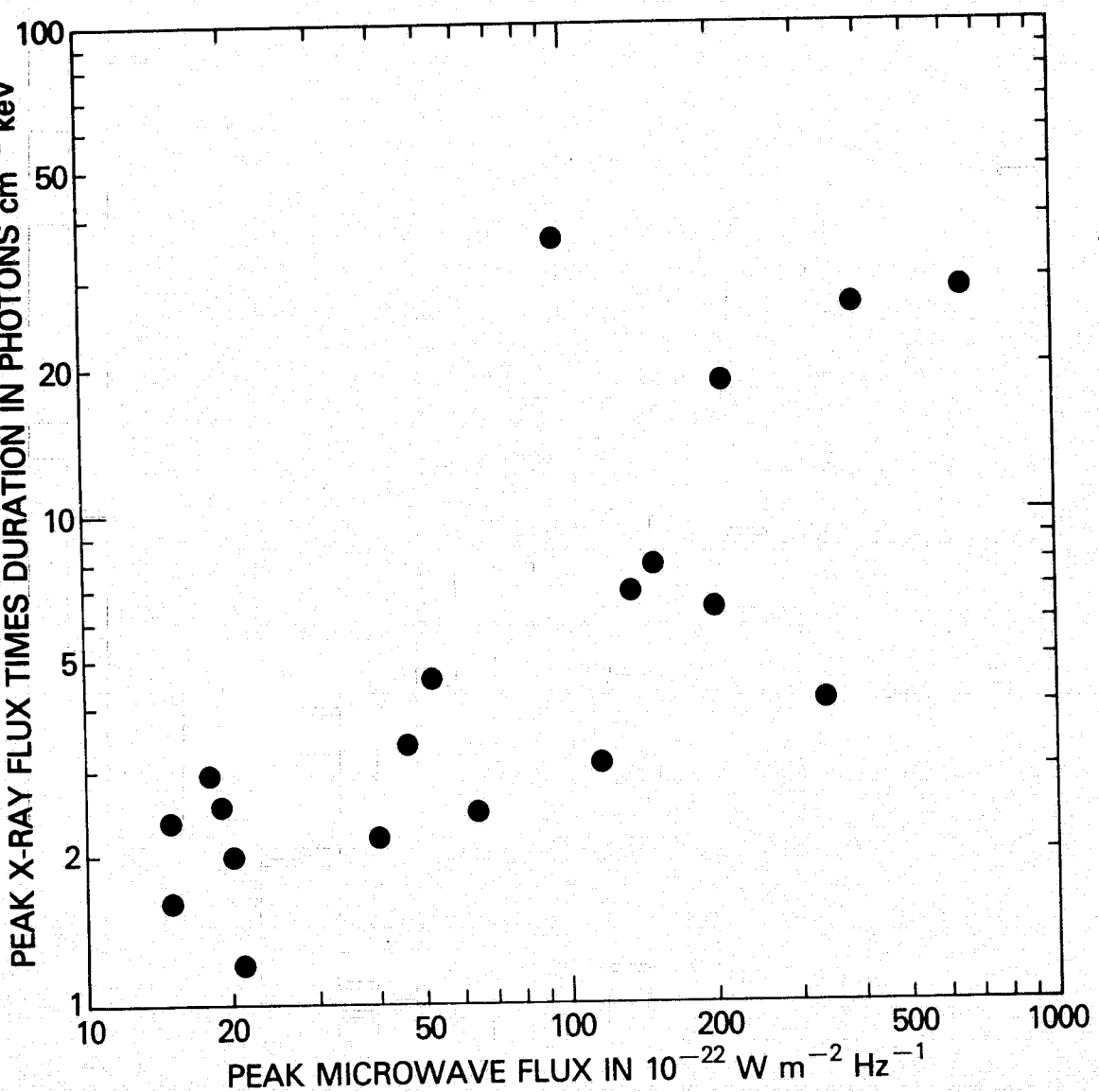

Figure 37. Scatter Plot of S_x t_x Versus S_μ.

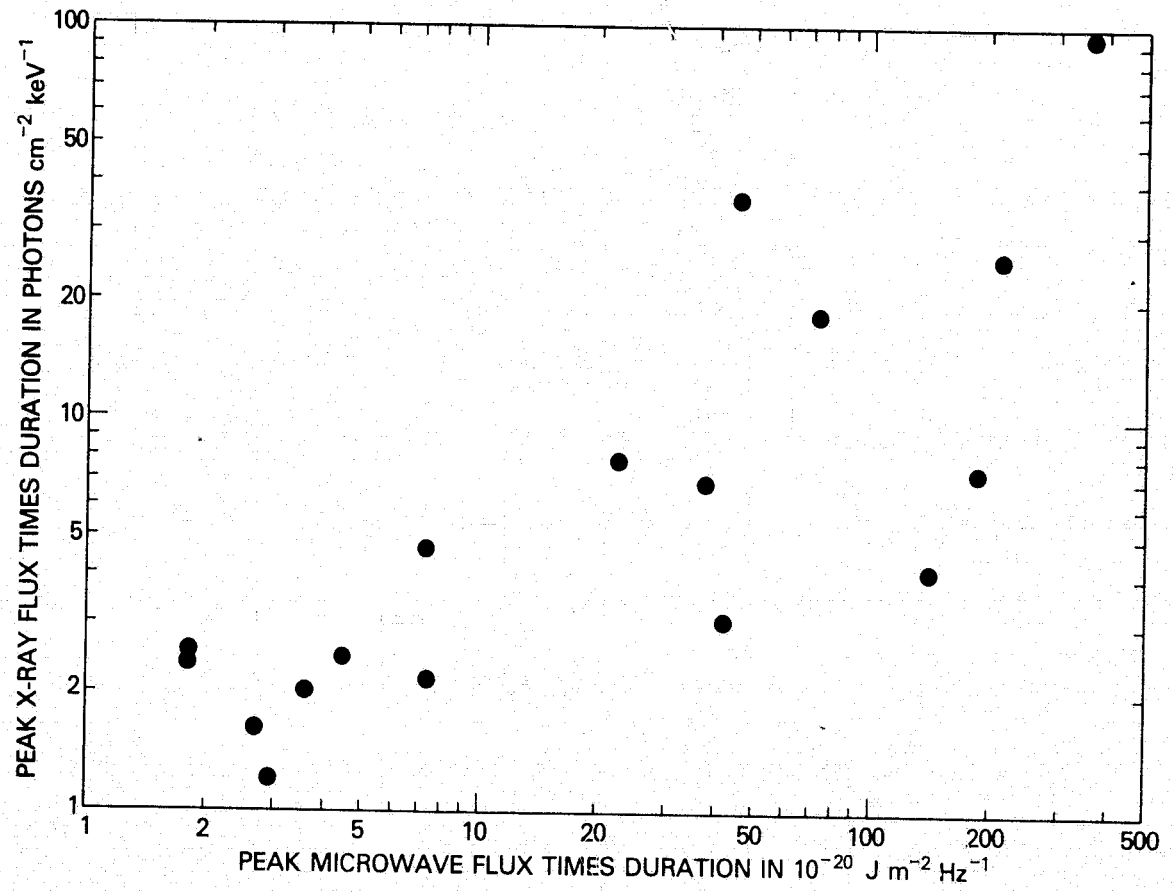

Figure 38. Scatter Plot of $S_x\ t_x$ Versus $S_\mu\ t_\mu$.

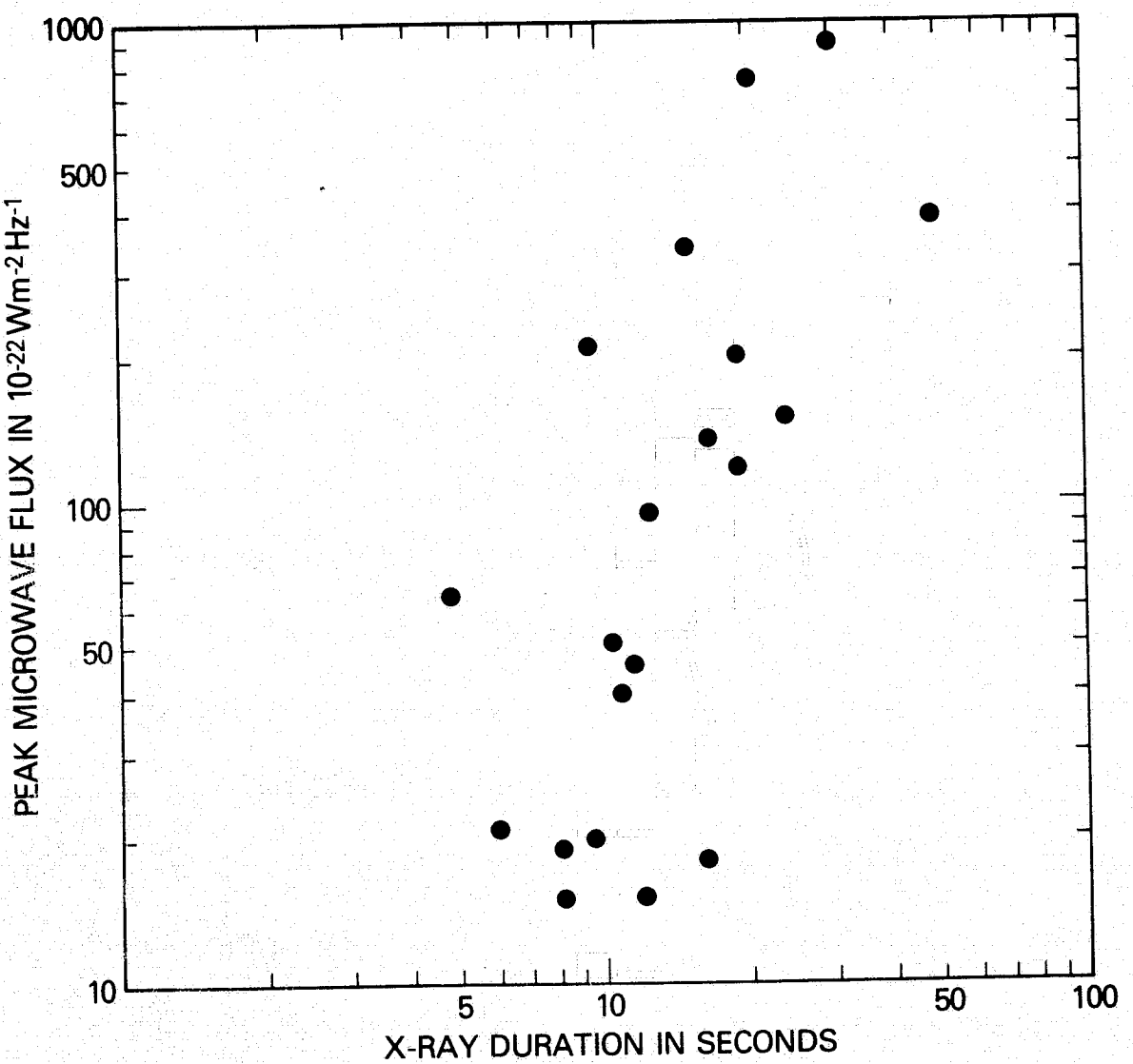

Figure 39. Scatter Plot of S_μ Versus t_x.

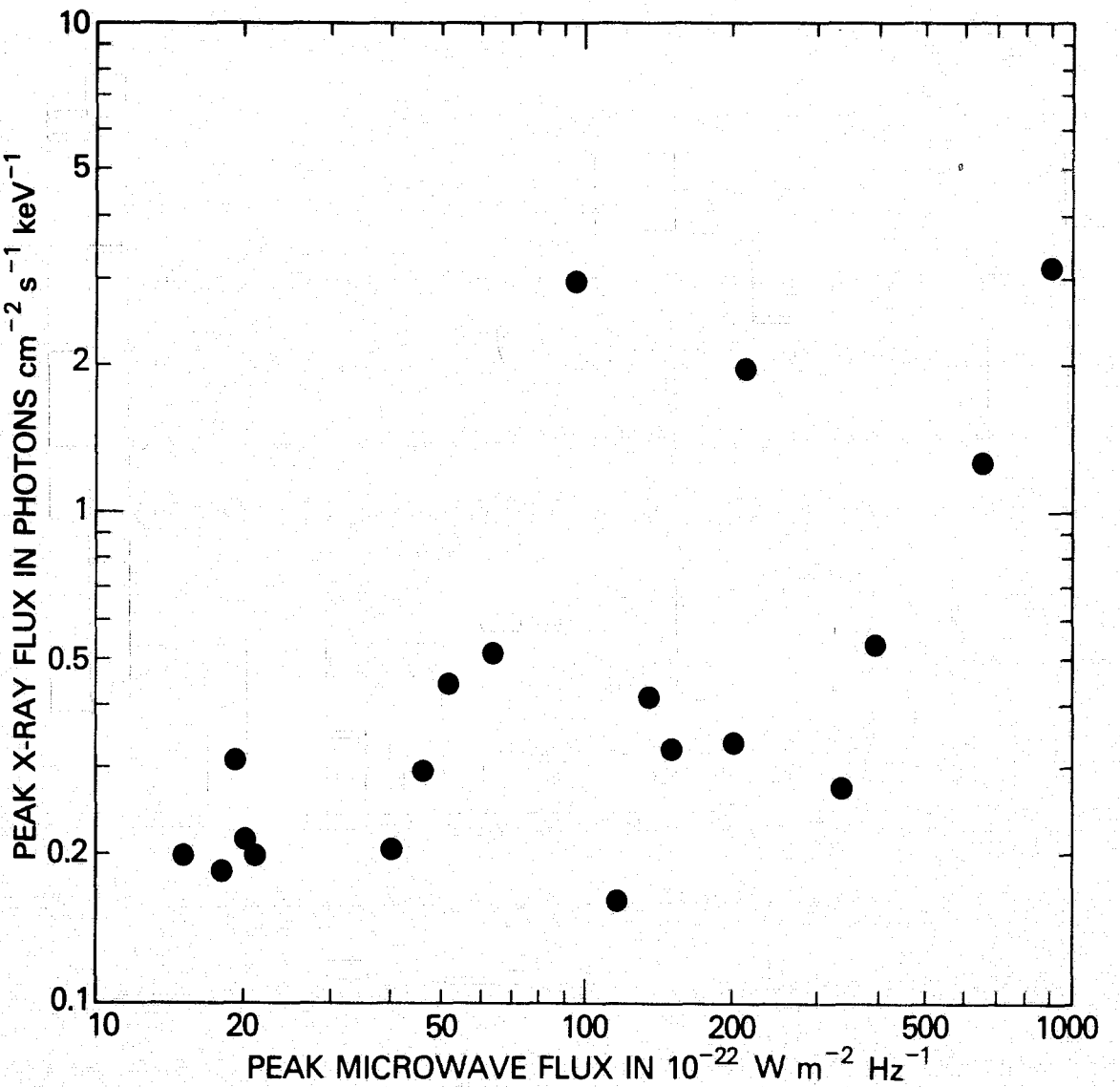

Figure 40. Scatter Plot of S_x Versus S_μ.

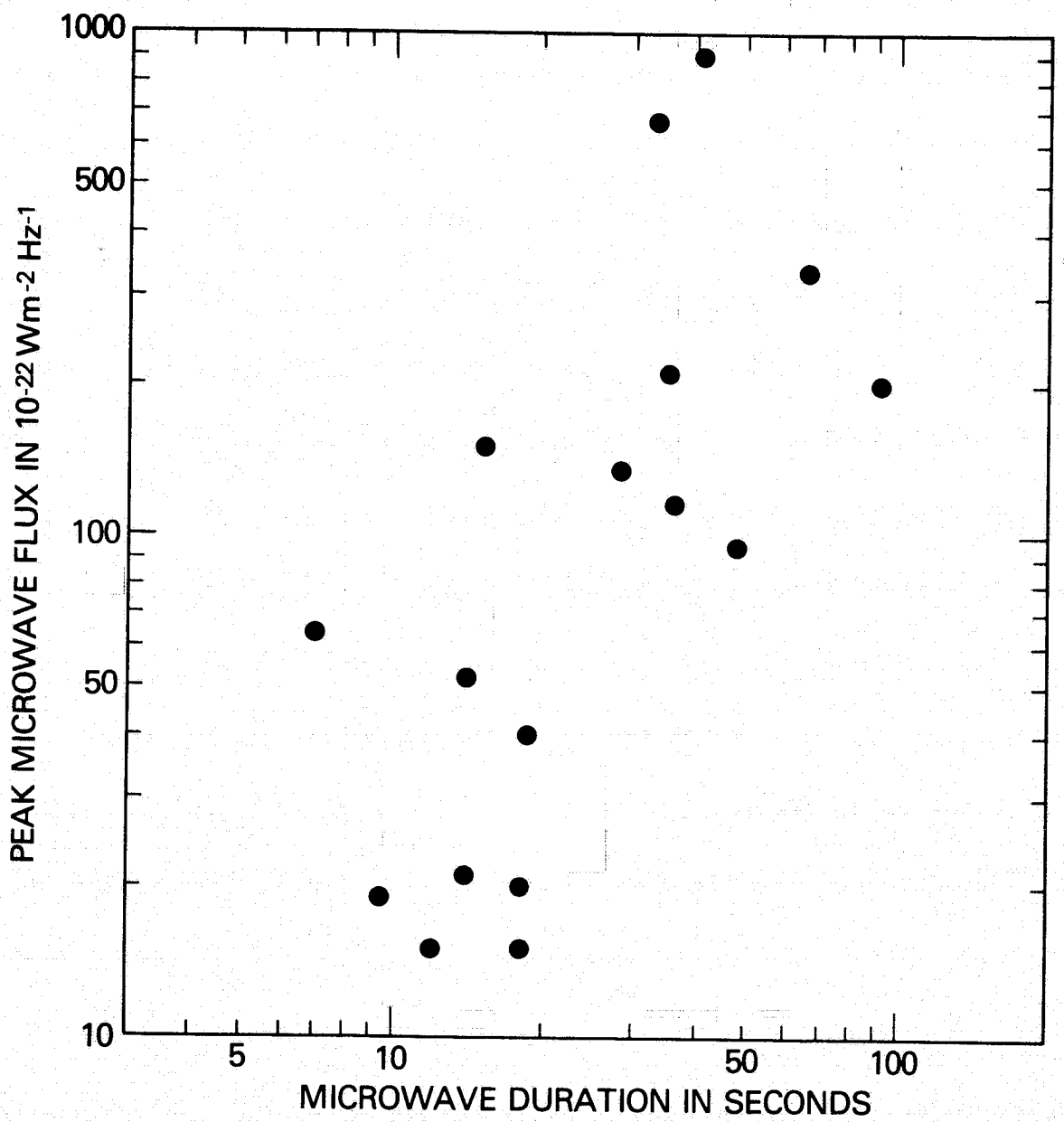

Figure 41. Scatter Plot of S_μ Versus t_μ.

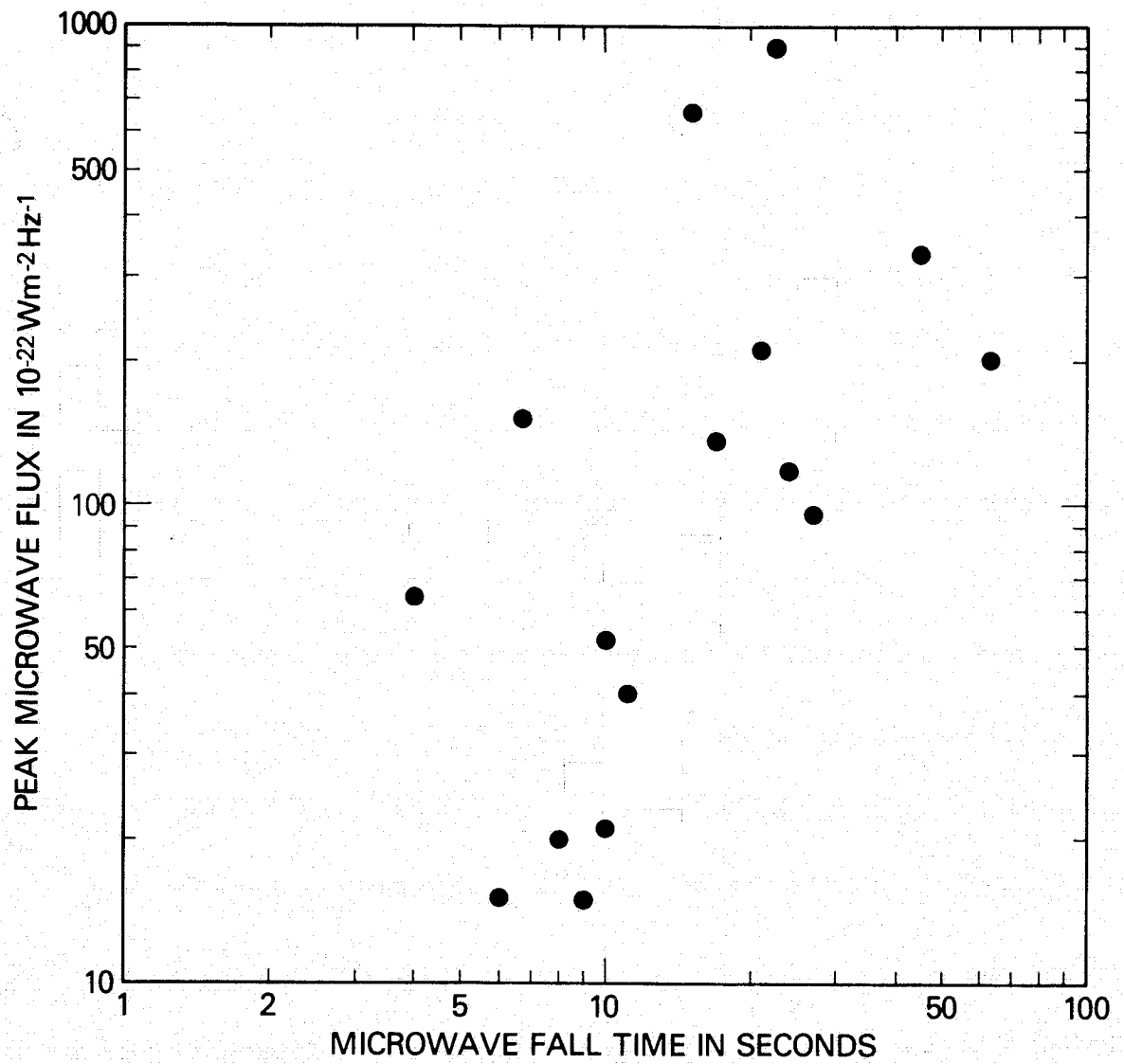

Figure 42. Scatter Plot of S_μ Versus $t_{\mu f}$.

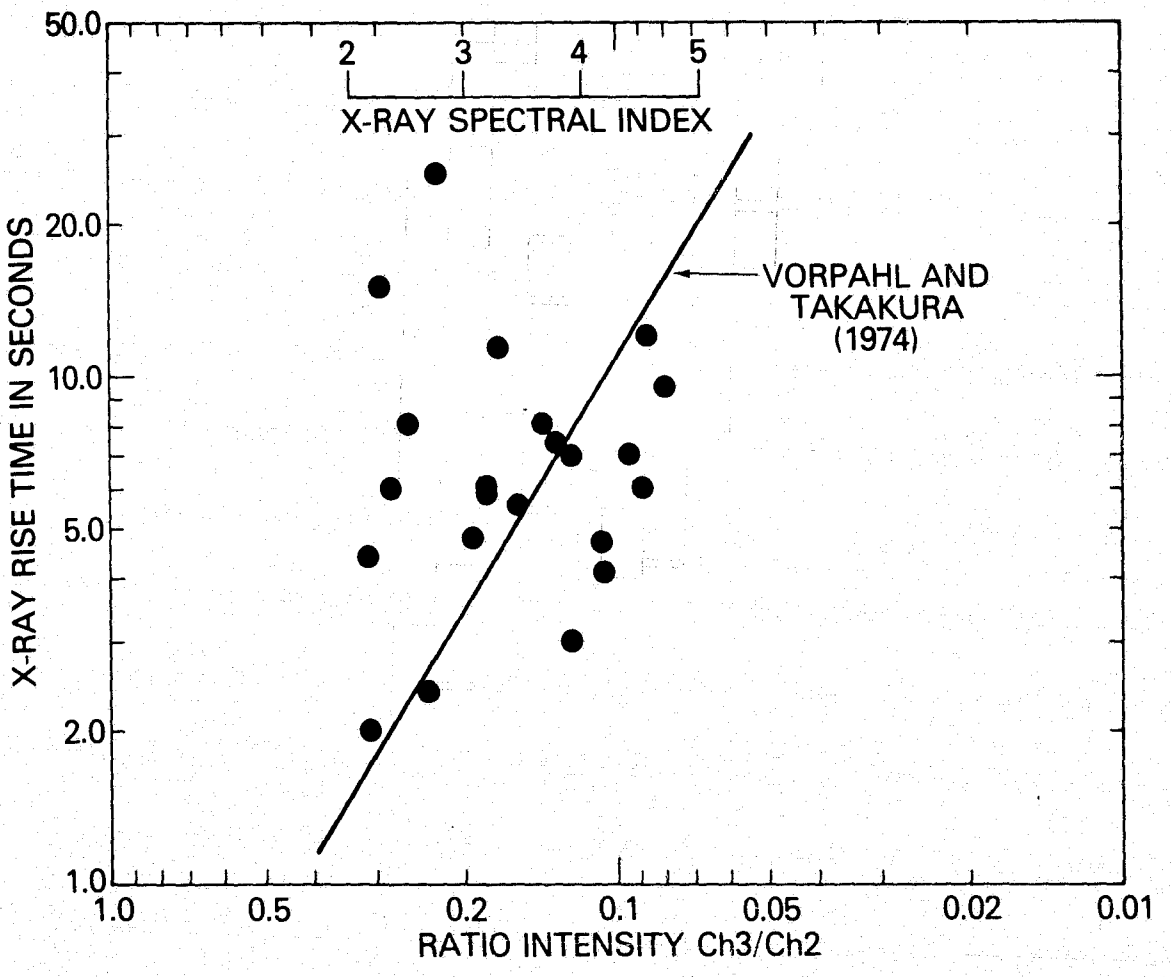

Figure 43. Scatter plot for data obtained in the present work together with the relationship found by Vorpahl and Takakura (1974).

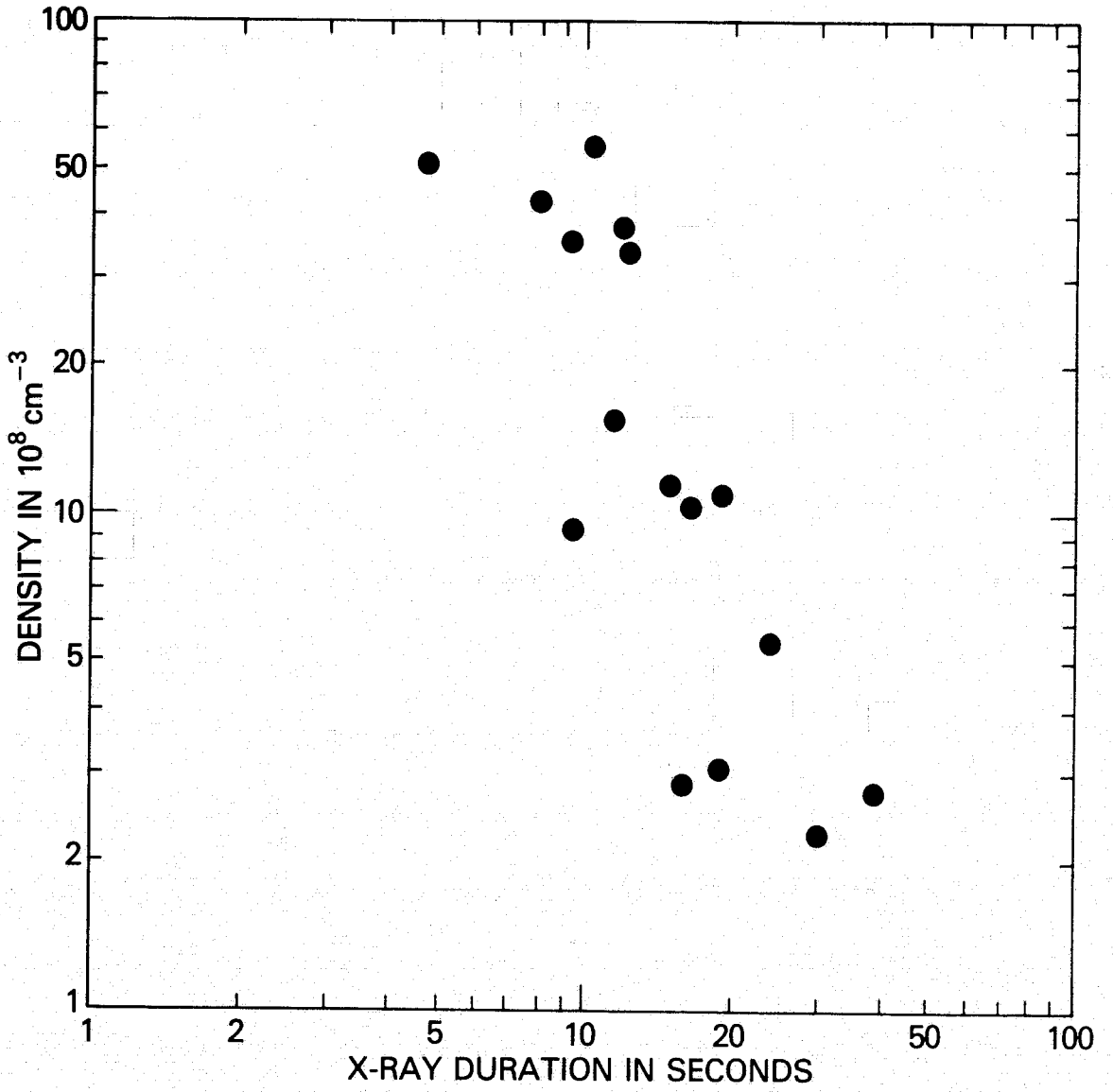

Figure 44. Scatter Plot of n_e Versus t_x.

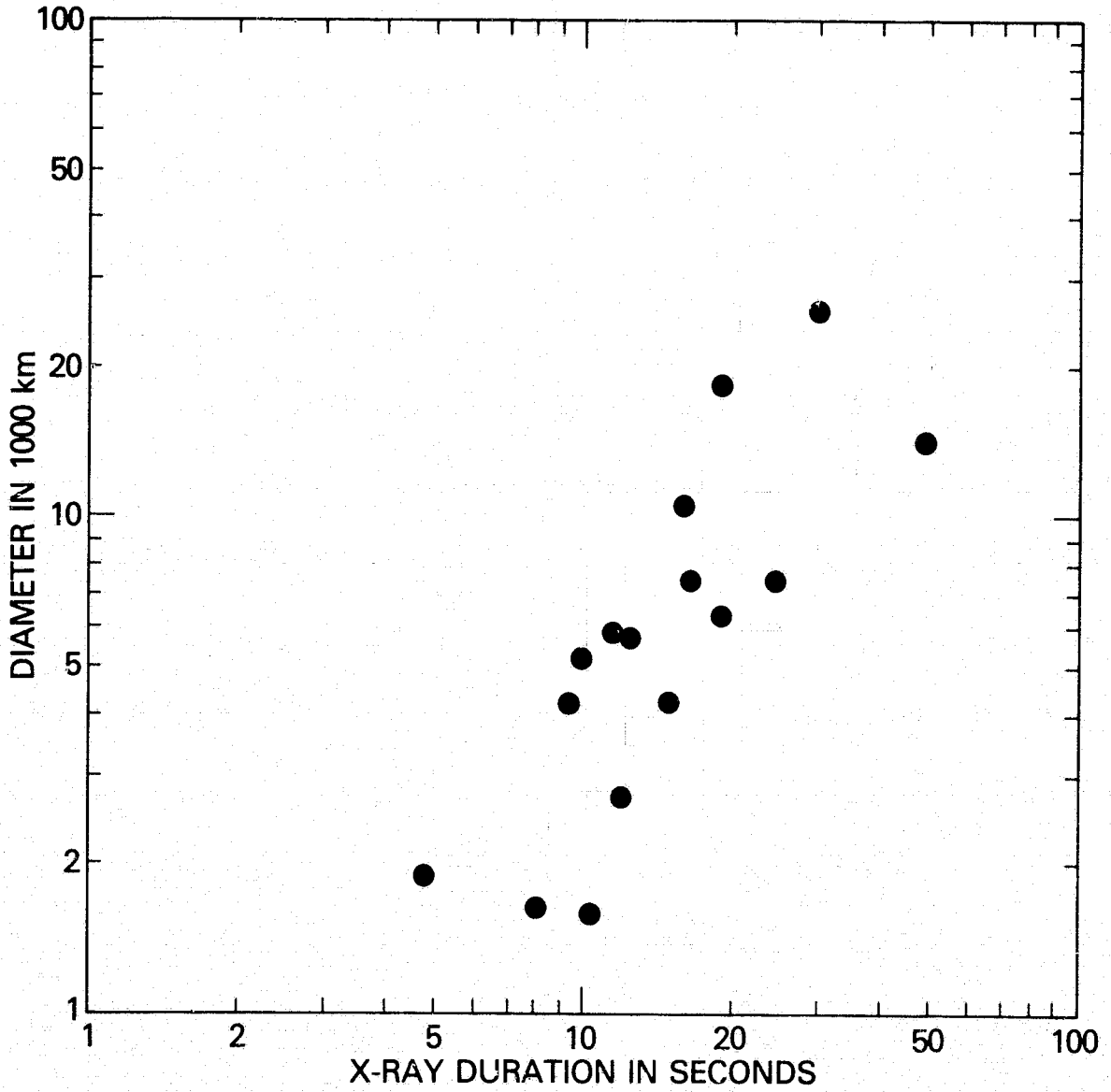

Figure 45. Scatter Plot of D Versus t_x.

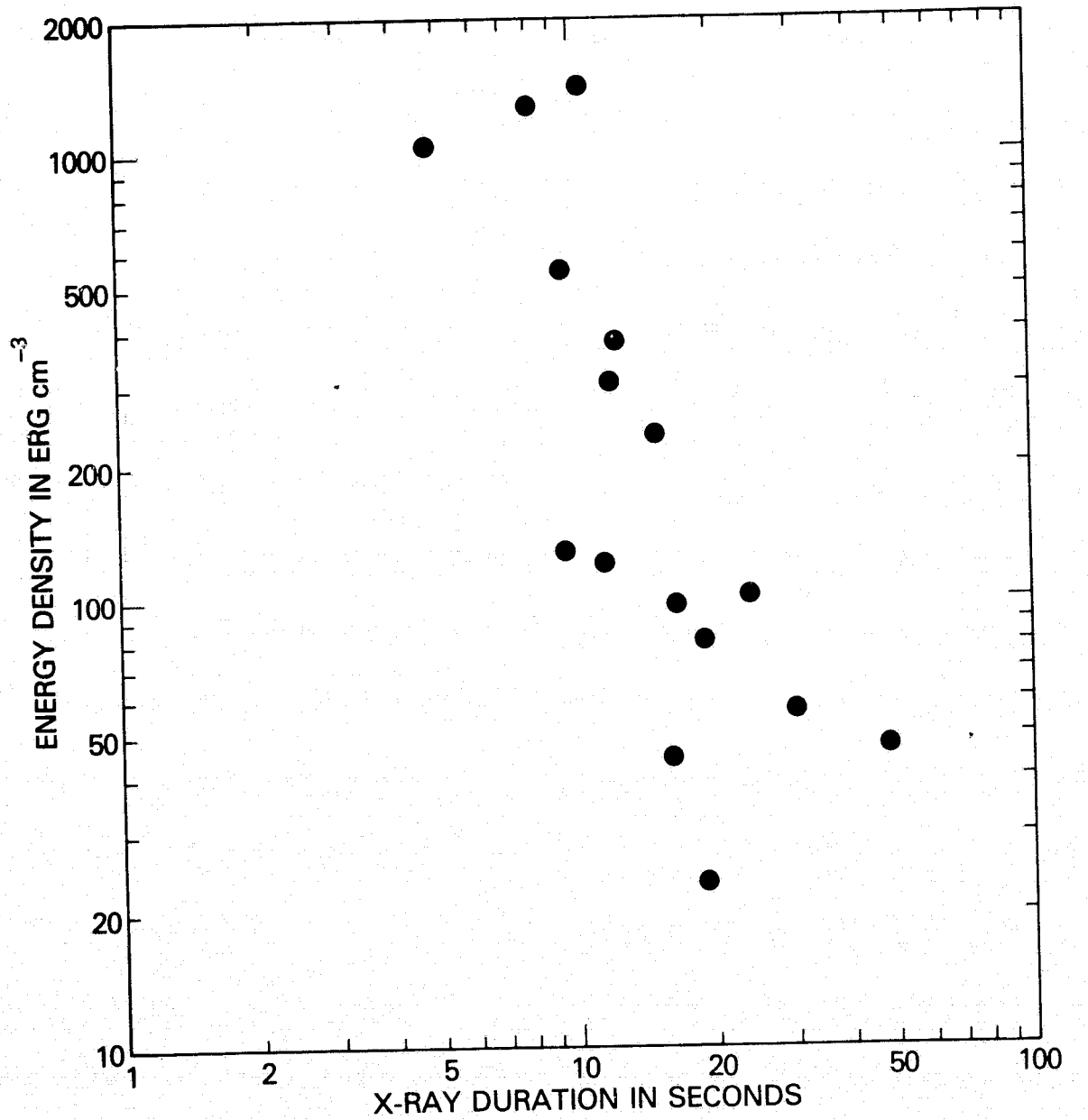

Figure 46. Scatter Plot of ED Versus t_x.

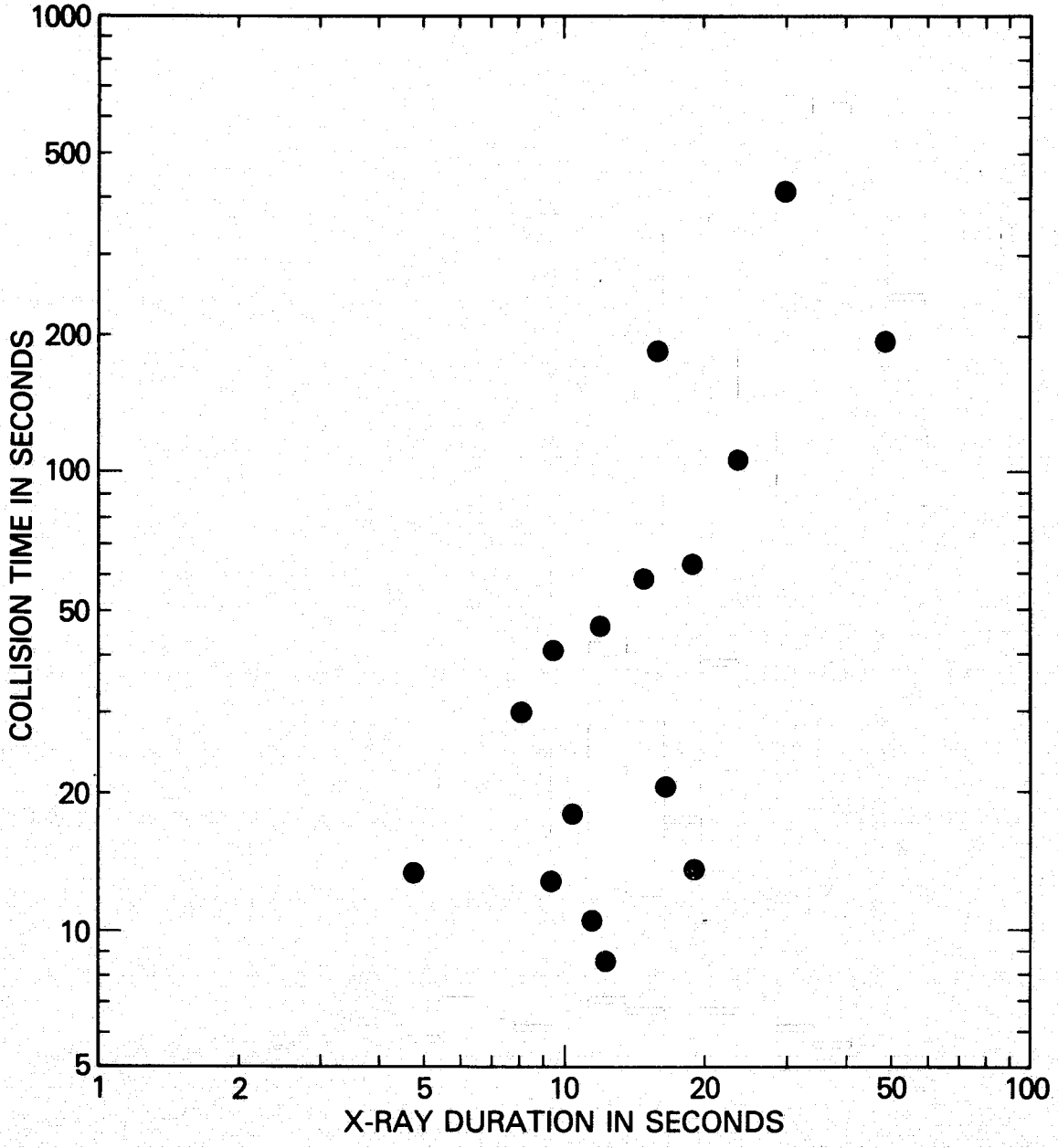

Figure 47. Scatter Plot of t_c Versus t_x.

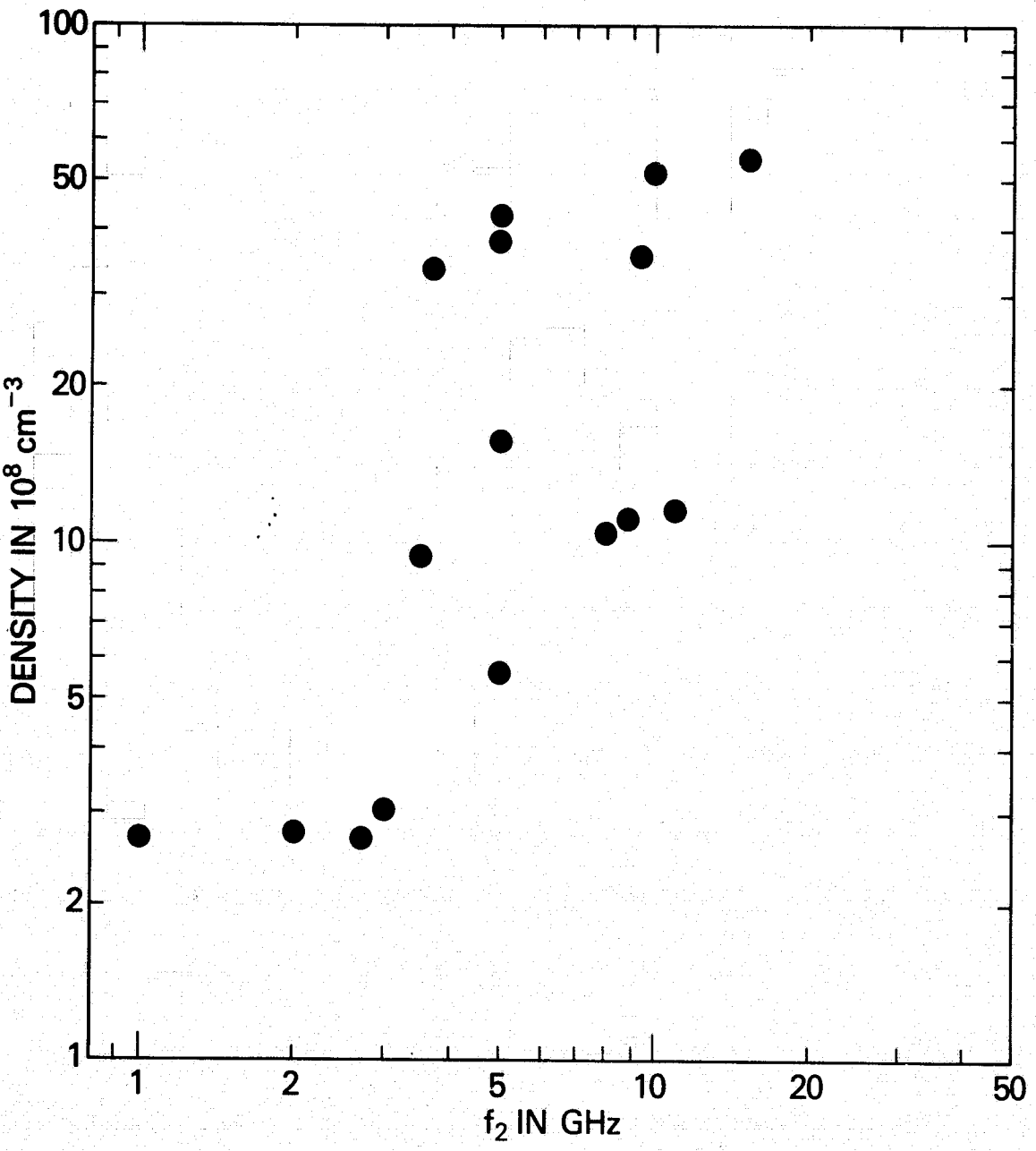

Figure 48. Scatter Plot of n_e Versus f_2.

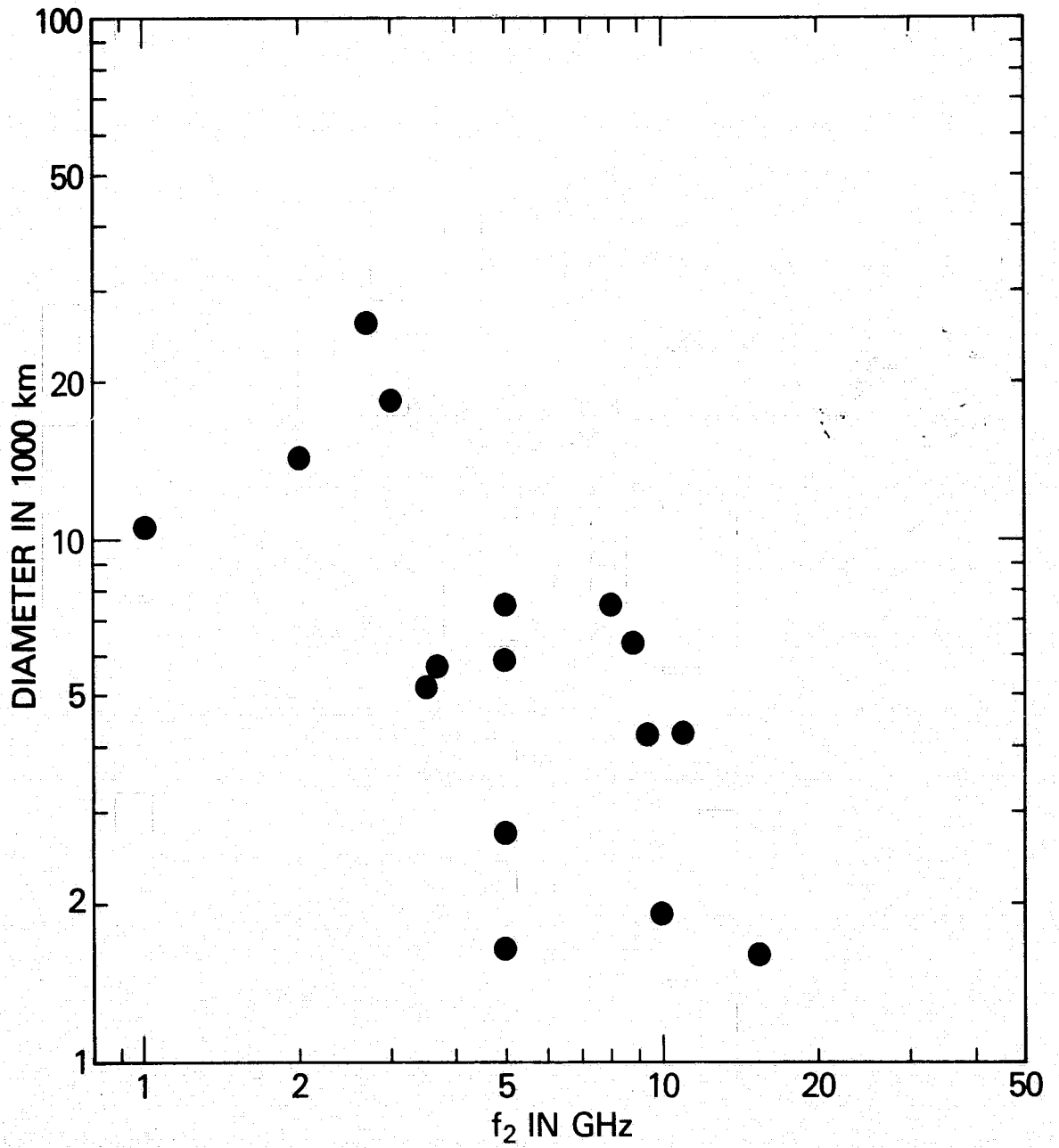

Figure 49. Scatter Plot of D Versus f_2.

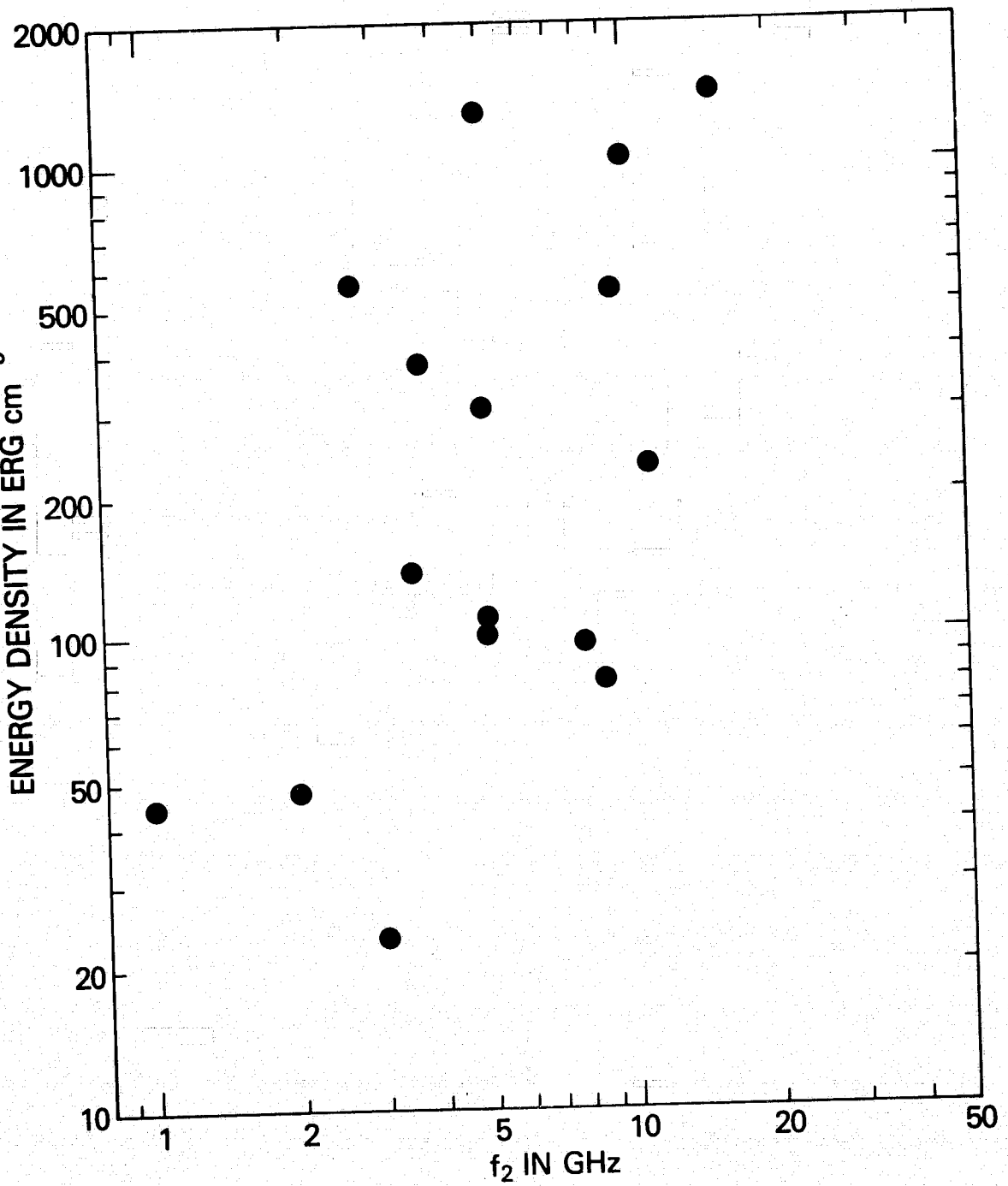

Figure 50. Scatter Plot of ED Versus f_2.

4. DISCUSSION

4.1. Instrumental, Observational, and Analytic Effects

The selection criteria described in the first section bias the set of events to be analyzed towards short-duration bursts because the more rapid the rise and the more rapid the fall of a burst, the less likely it is to exhibit significant departures from monotonic increase and decrease. The set is not biased, however, against events with rise times systematically longer or shorter than fall times. The reason that symmetric rise and fall of the hard X-ray burst is evident in the present work, but not reported in earlier studies of impulsive phenomena (Kane and Anderson, 1970), may be due to a difference in the energy range investigated. In the present work most of the X-ray flux is observed in Channel 2 or an energy range of 28 to 55 keV; while in the work of Kane and Anderson, the observed flux is dominated by the energy range 9.6 to 19.2 keV. This lower range may be strongly influenced by the soft X-ray emission not considered here.

The criterion defining the maximum allowable deviation from monotonic increase and decrease was chosen to select as clean a sample as was available in the OSO-5 data, while imposing as little bias as possible against large bursts. The choice of a limiting percentage deviation of ±15% satisfies the *Solar-Geophysical Data* designation of "simple" microwave bursts with "fluctuations" and encompasses the one standard deviation fluctuation in the peak counting rate of the smallest events.

The instrumental and analytic thresholds on the duration of an event and on the intensity of an event were completely decoupled so that the threshold criteria are not responsible for the lack of correlation between these two observational parameters. The absence of correlation between burst duration and peak intensity in hard X-rays is in apparent conflict with the correlation found between the analogous microwave parameters. Both results are, however, consistent with the adiabatic-heating model which is developed in Paper 2 to explain the spike burst observations. The correlation between burst rise time and spectral index reported by Vorpahl and Takakura (1974) is suggestive of instrumental difficulties with the observations which they analyzed. No such correlation is obtained in the present work based on the OSO-5 observations, in agreement with Hoyng (1975).

An effect of the energy resolution of the OSO-5 detector is to yield an apparent temperature, determined as described in Section III, which is between 1 and 2 2 keV greater than the temperature which characterizes the source spectrum. Spectral shapes for temperatures above 20 keV are not significantly distorted (cf. Paper 2).

The emission measure reported for each of the spike bursts is approximately linearly dependent on the efficiency factor determined for Channel 2 of the OSO-5 detector. The temperature is most strongly dependent on the midpoint energy of each channel. These energies enter as linear coefficients of the logarithms of the calculated flux densities in the determination of the mean temperature. The energy calibration of the detector was determined from preflight laboratory measurements and was continuously monitored inflight as described by Frost, et al. (1971). With the exception of Channel 1, within which the detection efficiency is a strong function of the incident photon energy, the absolute values of the midpoint energies are believed to be accurate to ±10%, including the calibration uncertainties, the temporal fluctuations, and the dependence on the shape of the photon spectrum. The midpoint energies of the channels relative to one another are significantly better known with uncertainties of order 1%. The detection efficiencies were determined from observations of the Crab Nebula with the OSO-5 detector as described by Dennis, et al., (1973). Independent determination of the detection efficiency of each channel was carried out by Enome (private communication) with similar results. These values are also consistent with the calculated efficiencies, including the effects of finite window thickness, attenuation length in the detector, detector resolution, and anticoincidence properties of the detector shield. The values of the efficiency factors, given in Table 1, are believed to be accurate to ±15%.

4.2. Implications and Interpretations of Results

4.2.1. Meterwave

The observations presented in Table 4 show that only two or possibly three of the spike bursts are associated with ordinary (non-reversing) type III emission, whereas four or possibly all five for which meterwave emission is reported are associated with U bursts. Three or possibly all five are associated with type V emission. In a study of meterwave emission and sunspot configuration, Fokker (1971) found U bursts associated with only 22% of the general type III bursts studied. Nevertheless, similar to the results reported here, Fokker found high rates of coincidence, ~40%, between U bursts and type V emission. The relatively high incidence of U bursts and type V emission in association with the simple impulsive spike bursts and with each other supports the hypothesis that the particles are confined in a closed magnetic field region, which is a necessary condition for the adiabatic model. The nonthermal meterwave emission may be the result of the interaction of particles in the transition region between the hot plasma and its environment. The infrequency of meterwave emission in association with the spike bursts (Kundu 1965) should again be emphasized by recalling that only 5 of the 21 events for which meterwave coverage was available reported any meterwave emission.

4.2.2. Microwave

As has been found in previous studies of microwave and hard X-ray emission from solar flares, the peak of the microwave emission tends to occur at very nearly the same time as the peak of the hard X-ray emission. This is illustrated in Figure 15. The most probable relationship is for the peak of the microwave emission to occur ~2 seconds after the peak of the hard X-ray emission. The close coincidence between microwave and hard X-ray emission is shown schematically in Figure 28 for the 17 spike bursts for which detailed microwave time studies are available. The two exceptions are Events Number 7 and Number 10, in which the peak microwave emission occurs 8 or more seconds later than the X-ray peak. The microwave emission also shows drift behavior, with the peak emission occurring later at lower frequencies, (cf. Figures 24 and 25); where no frequency drift can be identified in the remaining events. The anomalous events are discussed in more detail by Ohki (1977) together with additional events clearly showing features of frequency drift.

4.2.3. X-Ray Spectra and Spatial Parameters

The assumptions on which the derived parameters are based can be checked for internal consistency and for consistency with other solar flare observations. The assumption of single temperatures to characterize the spike bursts can be checked most readily for the five most intense bursts which exhibit statistically significant X-ray flux levels in the higher energy channels. The spectra during the rise, peak, and fall of each of these five bursts are shown in Figures 51 through 55. Deviations from an exponential or single-temperature spectrum are seen during the peak of Event Number 10 and also during the fall of several of the events. It should be noted, that each of these deviations is in the sense that the higher channels exhibit an excess flux over that expected for the temperature characterizing the fluxes observed in Channels 2 and 3. This same behavior can be seen in Table 5 for Event Number 7 from a comparison of the mean temperature with $T_{CH2/CH3}$. Only Events Number 7 and Number 10 show a significant deviation from a single temperature at the peak and in both instances the mean temperature is higher than that determined from the lower energy channels. These two events are anomalous in other respects as is noted in Subsection 4.2.2. The assumption of single temperatures is consistent with the spectra at the peak for 20 of 22 spike bursts. An interpretation of the two exceptional bursts and the excess high-energy flux observed during the fall of several of the events is presented in the following section.

The parameters presented in Table 6 depend not only on the assumption of a single temperature source for the X-ray and microwave emission but also on near spherical symmetry of the source region. The values found for size,

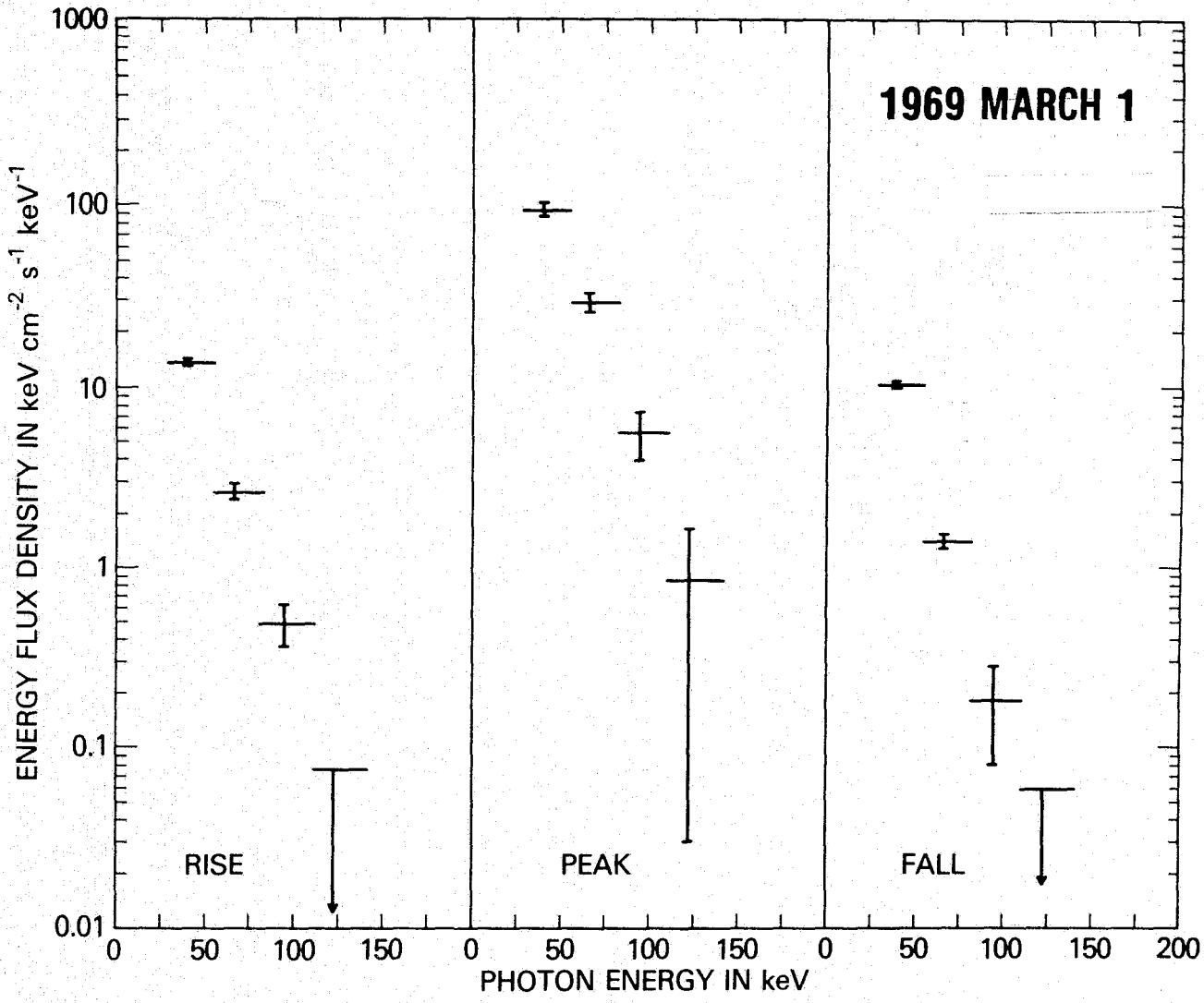

Figure 51. X-ray spectra during the rise, at the peak, and during the fall of Event Number 2.

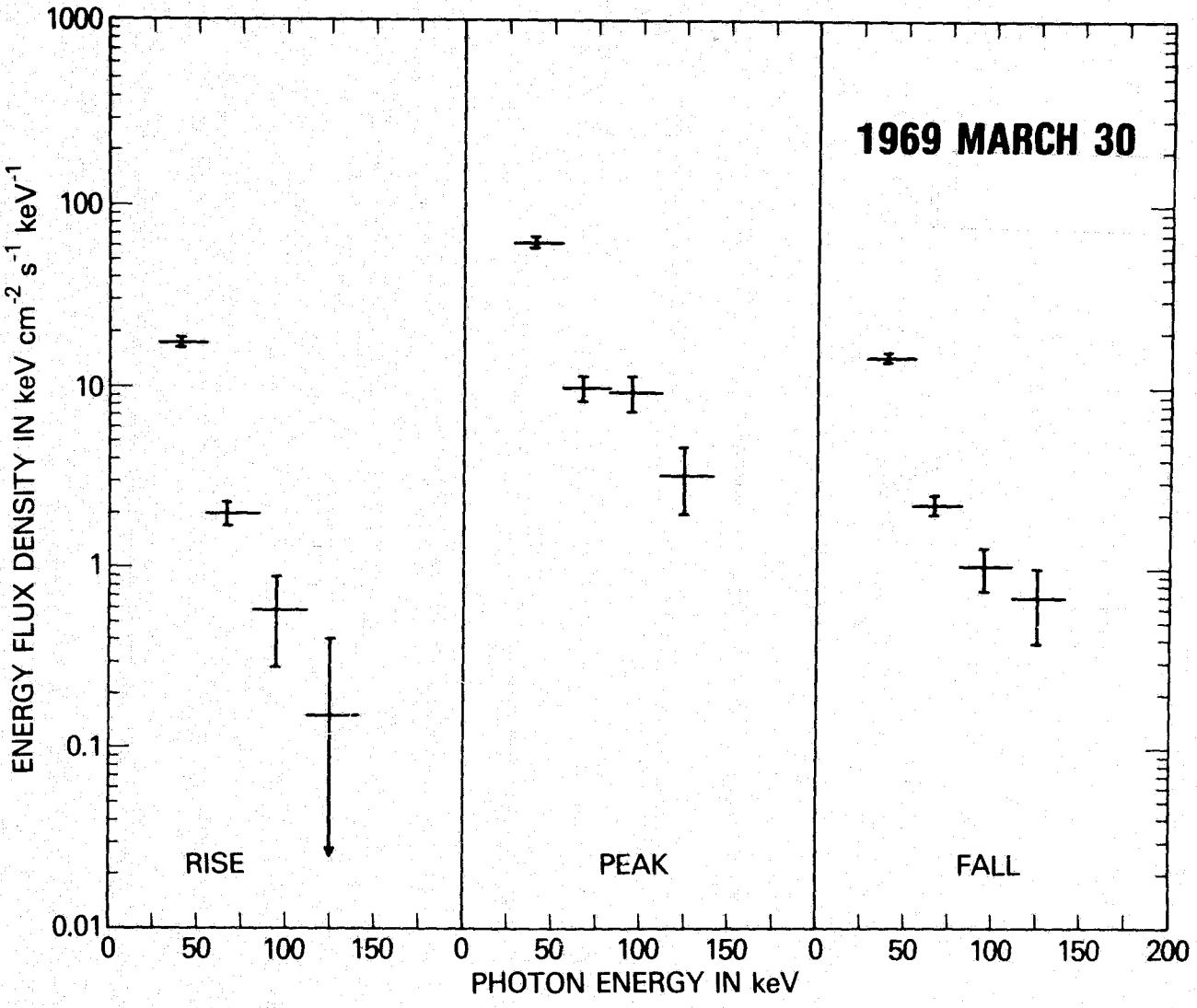

Figure 52. X-ray spectra during the rise, at the peak, and during the fall of Event Number 10.

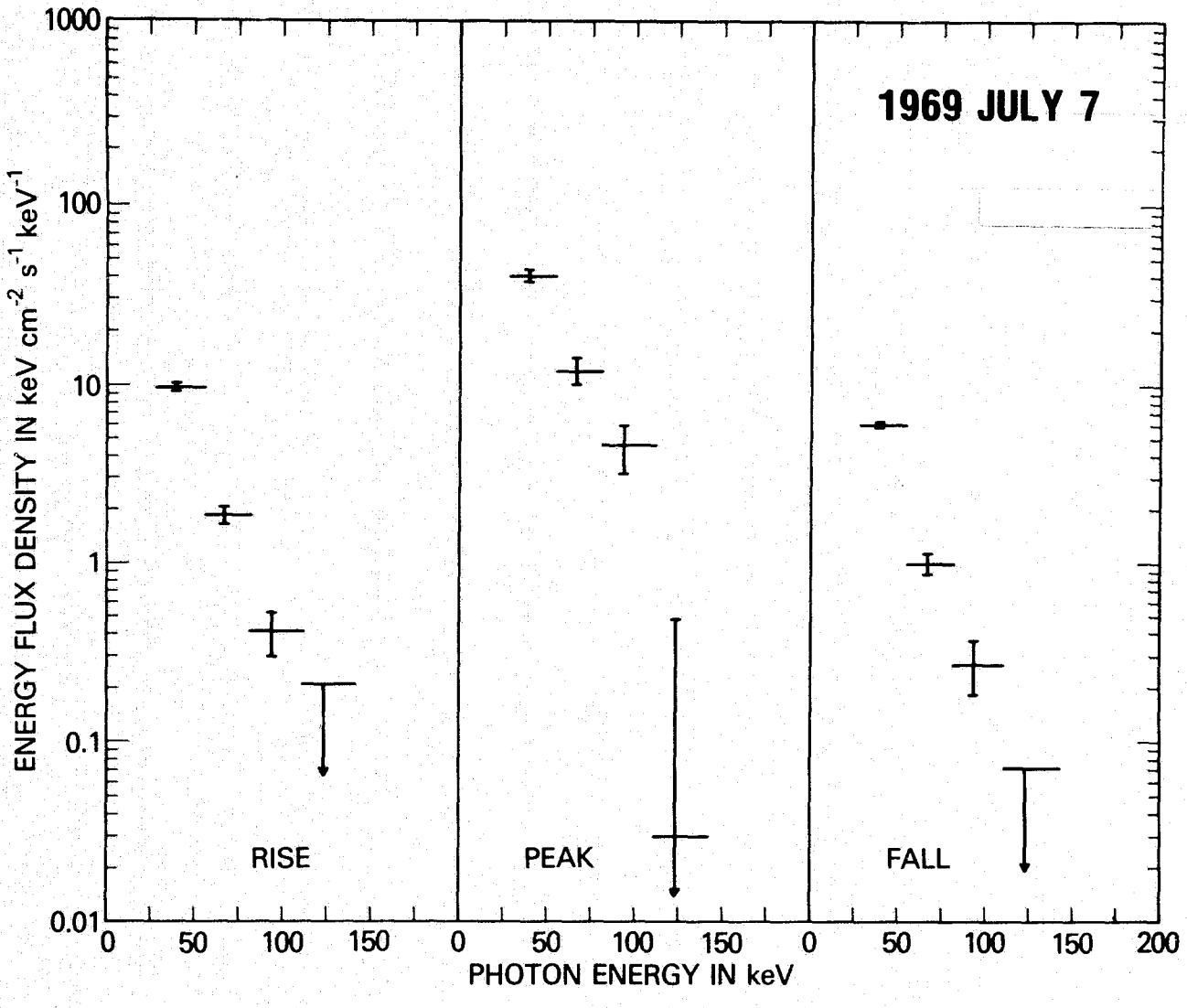

Figure 53. X-ray spectra during the rise, at the peak, and during the fall of Event Number 11.

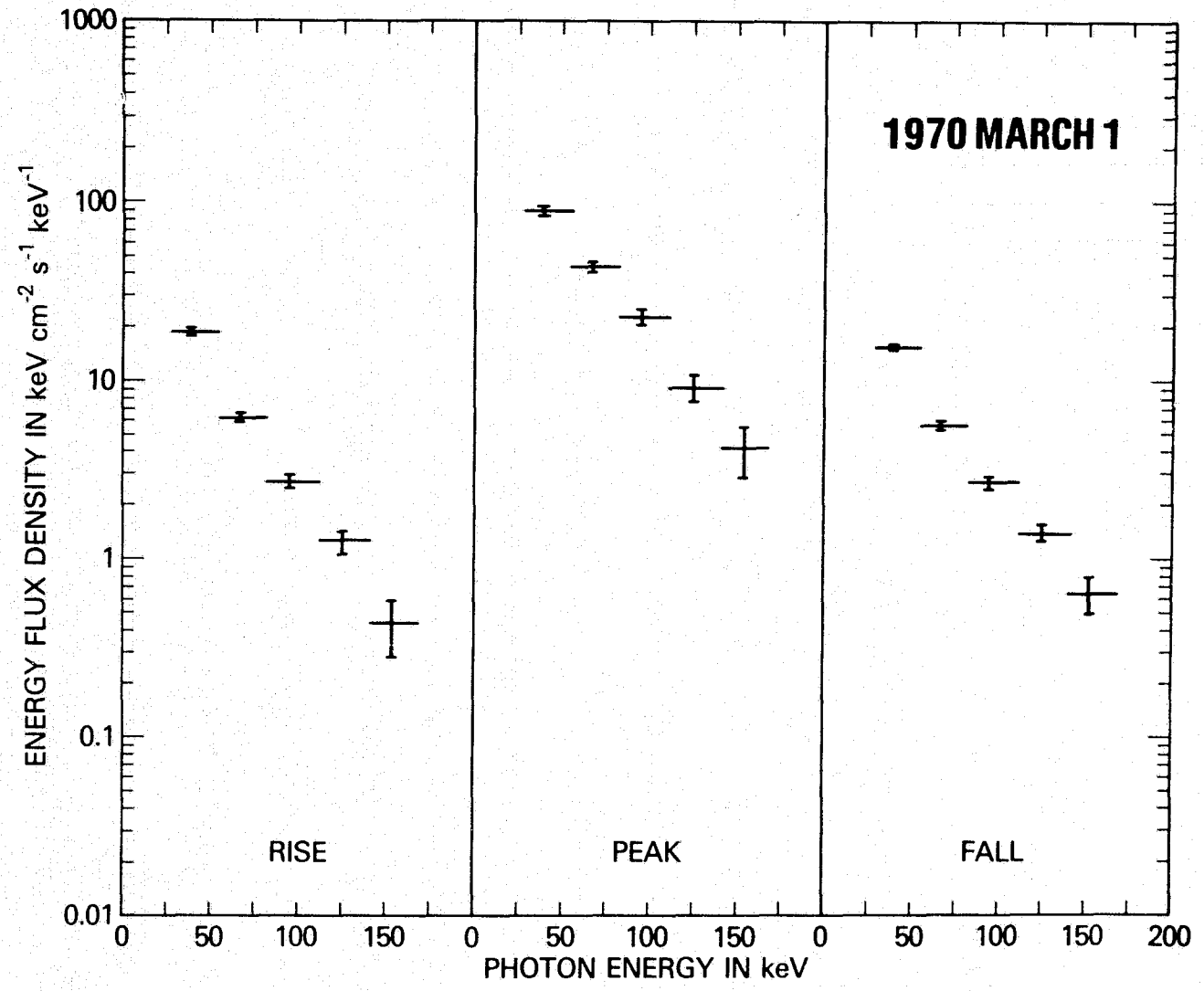

Figure 54. X-ray spectra during the rise, at the peak, and during the fall of Event Number 12.

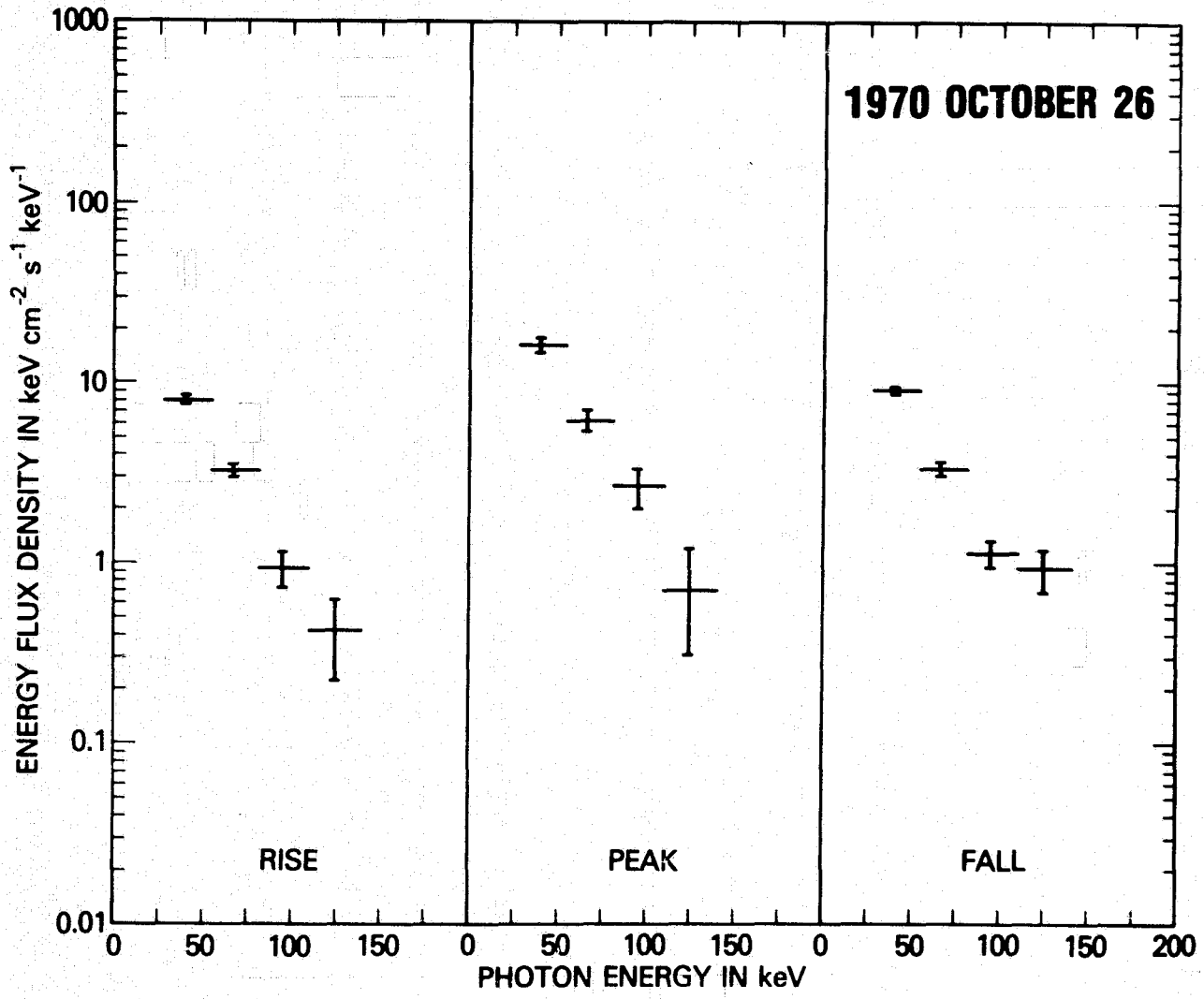

Figure 55. X-ray spectra during the rise, at the peak, and during the fall of Event Number 18.

density, and energy are reasonable for source regions in the lower corona and are corroborated by coincident observations. For example, the plasma frequency corresponding to the density calculated for Event Number 17 lies within the range of observed frequencies of the simultaneous decimetric emission shown in Figure 33. The results are attractive also because with the assumption of a common source there is no discrepancy between the number of electrons producing the observed X-ray emission and the number producing the microwave emission.

4.2.4. Correlations

In addition to the correlation observed between the X-ray rise time (t_{xr}) and the X-ray fall time (t_{xf}), temporal correlations were found as well between the microwave rise time ($t_{\mu r}$) and the microwave fall time ($t_{\mu f}$) and between the X-ray and microwave rise times. The correlation between t_{xr} and $t_{\mu r}$, together with the near coincidence between X-ray and microwave peak times, suggest a common origin for the two emissions. The symmetry between t_{xr} and t_{xf} suggests that whatever mechanism governs the increase in the observed X-ray flux also governs the decrease of these impulsive bursts. In such a case, the falling portion of the burst is not an independent, dissipative decay but rather a "turn-off" in the same sense that the rising portion of the burst is a "turn-on." In contrast with the X-ray time profiles, the temporal profiles of the microwave emission are not symmetric, even though the correlation between $t_{\mu r}$ and $t_{\mu f}$ is of nearly the same statistical significance as the correlation between t_{xr} and t_{xf}. Another result which is at first surprising is that t_{xf} and $t_{\mu f}$ are not correlated even though each of these fall times is correlated with the corresponding rise times which are, in turn, correlated with each other. The linear least-squares fits given in Table 7 for these temporal parameters yield the relationship $t_{xr} \approx t_{xf} < t_{\mu r} < t_{\mu f}$. If the shortest observed time intervals, t_{xr} and t_{xf}, characterize the fundamental mechanism energizing the impulsive solar flares, then $t_{\mu r}$ depends on the energizing process and some other factor. Because $t_{\mu f}$ is correlated with $t_{\mu r}$ but not with either t_{xr} or t_{xf}, $t_{\mu f}$ must depend primarily on the other factor rather than on the energizing process. The other factor may also explain the delay of the microwave peak with respect to the peak X-ray emission. In this context, Events Number 7 and Number 10 may be understood as extreme examples in which the other factor not only dominates the observed microwave emission but also influences the X-ray emission to the extent of modifying the observed spectrum.

The most significant correlation based on the observed intensities and temporal parameters is between the peak microwave intensity S_μ, and the product of the peak X-ray intensity S_x, with the X-ray duration, t_x. This correlation is in one sense the reverse of the relationship found by Neupert (1968) between the microwave emission and the soft X-rays observed in a more general class of solar

flares. In that study the soft X-ray flux was found to be proportional to the time integral of the microwave flux within a burst, but no correlation from burst to burst was established. In the present work, correlations are found as well between the product $S_\mu t_\mu$ and the product $S_x t_x$, and also between the peak intensities S_μ and S_x. The differences in the statistical significance of these correlations appear to be real; they may be understood in the context of the two factors controlling the temporal structure of the X-ray and microwave emissions if the unexplained factor is a time integral over the factor associated with the fundamental energizing process. All three correlations, nevertheless, suggest a common origin for the microwave and X-ray emission.

As has been found in a number of earlier studies (Cribbens and Matthews 1969, Cliver et al. 1976, Wiehl 1977, and D. Neidig, private communication), the duration or period of the microwave burst is well correlated with the peak microwave intensity. For the spike bursts, the peak microwave intensity is found not only to be correlated with the measured microwave duration but specifically to be correlated with the microwave fall time and not correlated with the microwave rise time. These results further indicate that the microwave intensity and fall time are influenced predominantly by a flare component which is not a dominant influence on the microwave rise. The duration of the X-ray burst is not correlated with the peak X-ray intensity but is correlated with the peak microwave intensity. The correlation between S_μ and t_x is even stronger than the correlation between S_μ and t_μ.

Four significant correlations were found between the duration of the X-ray spike bursts and the derived parameters. All of these parameters depend on the flare area which is derived from the X-ray and microwave spectra at peak emission. The correlation between X-ray burst duration and size (t_x and D) is consistent with any model in which the flare particles are energized by a macroscopic disturbance of the whole flare region so that the duration is determined by the time in which the disturbance can traverse the flare source (Uralov and Nefed'ev 1976). The mean velocity given by the correlation between burst duration and diameter is $\sim$500 km s^{-1}, typical of observed motions in flare plasmas.

Unlike any of the other correlations, the correlations between f_2 and the other derived parameters may be artifacts of the analysis. As indicated by Equations (9) through (13), f_2 enters into the calculation of each of the parameters for which a correlation with f_2 is found to be statistically significant. No physical significance is attached to these correlations as a result of the present work.

The lack of correlation between the observed Hα area and the area calculated for the peak emission in the present work agrees with the suggestion of Zirin (1966) that the extent of Hα emission may be unrelated to the region of primary energy release.

5. CONCLUSIONS

Focusing the analysis of solar-flare phenomena on the simple impulsive spike bursts has produced some surprising but clear results. The strength of the present study is derived primarily from the availability of coincident high-energy X-ray and microwave observations with good time resolution. Consequently most of the new insights are based on the temporal behavior of the radiation. The most striking new result is the symmetry found in the temporal profiles of the X-ray emission. The fact that the X-ray emission turns off with the reverse of the time structure with which it turns on strongly suggests a causal mechanism which is reversible. The simplest energizing process which satisfies this requirement is heating by an adiabatic compression followed by expansion and cooling. To test the hypothesis that such a mechanism is responsible for the observed emission, flare parameters have been derived from the observational data based on the assumption that the X-ray and microwave emission originate from the same single-temperature source. The spectra of the observed X-ray and microwave emission, as well as their generally correlated intensities and temporal behavior, support this hypothesis. Fine details in the temporal and spectral characteristics of the spike bursts, however, require additional explanation.

The existence of an additional process influencing the microwave emission is indicated by many of the observations. These include the delay of the microwave peak with respect to the X-ray peak emission, the longer fall time of the microwave emission, the lack of correlation between the microwave and the X-ray fall times, and the strong correlation between the peak microwave intensity and the product of the peak X-ray intensity with the X-ray duration. These observations also suggest that the process is dependent on the time integral of the primary process which determines the X-ray emission. Leakage of energetic electrons out of the primary source region could produce just such an effect if they escaped into a cooler, less dense region, not optically thick to the microwave emission. The efficiency with which escaping electrons produce observable microwave radiation is greatly enhanced by the lack of self-absorption. On the other hand, the escaping electrons would be relatively inefficient emitters of bremsstrahlung radiation in the less dense medium. It is with respect to the leakage process that Events Number 7 and Number 10 and the falling portions of the most intense bursts could be extreme cases. Leakage of a large fraction of the source electrons, primarily those with the highest energies, could account for the observed distortions of the X-ray spectrum and the frequency drift of the microwave radiation. The existence of two processes determining the microwave emission, only one of which dominates the observed X rays, would explain why burst duration and peak microwave intensity are correlated, whereas burst duration and peak X-ray intensity are not. The peak microwave flux may include a significant contribution from the total number of leaked electrons which depends, in turn, on the duration of the X-ray burst.

Another entirely new result of the present work is the correlation between the duration of the X-ray emission and the size of the source region determined at the time of peak microwave emission. The velocity, calculated from the diameter and duration of the spike bursts, lies in the range from 200 to 700 km s^{-1}. Because this is a reasonable range of velocities within the solar atmosphere, the correlation supports the possibility that a compressional disturbance could traverse the source region and cause the required heating on time scales consistent with the time structures of the observed emissions.

Non-thermal models of impulsive solar flares have not been ruled out by the results of this study, but they are found lacking in that none of them incorporates a mechanism to explain the observed symmetry or the details of the correlations between the X-ray and the microwave emissions. Further tests of the adiabatic heating model are discussed in Paper 2 and may come from attempts to understand the impulsive components of complex solar flares. As discussed in the previous section, studies of microwave emission from complex bursts have shown a number of interesting correlations. Studies such as these, but with coincident X-ray observations, are needed so that complex bursts can be resolved into components and then analyzed with the parametric techniques developed here. The types of observations which would provide the most definitive tests of the assumptions on which the present analysis is based are those which combine spatial resolution with spectral and temporal resolution comparable to or better than that currently available.

In order to stress again the value of coincident observations, it should be noted that for any event without coincident X-ray and microwave observations *NONE* of the derived parameters presented in Table 6 and only half the parameters in the preceding table could have been calculated.

ACKNOWLEDGMENTS

The authors gratefully acknowledge M. A. Smith and J. W. Warwick, Boulder; S. F. Smerd, Calgoora; B. Kramer, Dwingeloo; A. Maxwell, Harvard; and H. Urbarz, Weissenau for sending us records of the dynamic spectra observed in coincidence with the spike bursts; and T. Janssens, Aerospace Corporation; A. Magun, Bern; B. Kramer, Dwingeloo; F. Yamashita, Hiraiso; M. Ishitsuka, Huancayo; A. E. Covington, Ottawa; J. Castelli, Sagamore Hill; D. L. Croom, Slough; and S. Enome, Toyokawa for sending us records of the fixed-frequency time profiles obtained in coincidence with the spike bursts. We also acknowledge the personnel of COMTECH, Edwin P. Cutler in particular, for assistance with the OSO-5 data management and reduction. We sincerely thank Judy Karpen and Herbert Wiehl for critical reading of this manuscript and Judy Karpen additionally for assistance in its preparation. The preparation of this manuscript was

carried out while two of us, Carol Jo Crannell and Christian Mätzler, were participants in the Skylab Solar Workshop on Solar Flares. This work comprises part of our contribution to the Workshop and the investigations undertaken by the Impulsive Phase Group. The stimulation and the opportunities for discussion and exchange of ideas provided by the Workshop are sincerely appreciated. The Skylab Solar Workshops series are sponsored by NASA and NSF and are managed by the High Altitude Observatory, National Center for Atmospheric Research.

REFERENCES

van Beek, H. F., de Feiter, L. D., and de Jager, C. 1974, Correlated Interplanetary and Magnetospheric Observations, Edited by D. E. Page, D. Reidel Publishing Company, Dordrecht.

Benz, A. O. 1977, Astrophys. J. 211, 270-280.

Bevington, P. R. 1969, Data Reduction and Error Analysis for the Physical Sciences, McGraw-Hill, New York.

Cliver, E. W., Hurst, M. D., Wefer, F. L., and Bleiweiss, M. P. 1976, Solar Phys. 48, 307-320.

Craig, I. J. D. and Brown, J. C. 1976, Nature 264, 340-342.

Cribbens, A. H. and Matthews, P. A. 1969, Nature 222, 158-159.

Datlowe, D. W., Elcan, M. J., and Hudson, M. S. 1974, Solar Phys. 39, 155.

Dennis, B. R., Suri, A. N., and Frost, K. J. 1973, Astrophys. J. 186, 97-107.

Drummond, W. E. and Rosenbluth, M. N. 1960, Phys. Fluids 3, 45-51 and 491.

Drummond, W. E. and Rosenbluth, M. N. 1963, Phys. Fluids 6, 276-283.

Flückiger, K. 1973, Proceedings of the Third Meeting of the Committee of European Solar Radio Astronomers (C. E. S. R. A.), Edited by J. Delannoy and F. Poumeyrol, FLOIRAC, Bordeaux, 134-138.

Fokker, A. D. 1972, Proceedings of the Second Meeting of the Committee of European Solar Radio Astronomers, Edited by A. Abrami, Trieste, 110-112.

Frost, K. J. 1969, Astrophys. J. 158, L159-L163.

Frost, K. J. and Dennis, B. R. 1971, Astrophys. J. 165, 655-659.

Frost, K. J., Dennis, B. R., and Lencho, R. J. 1971, New Techniques in Space Astronomy, Edited by Labuhn and Lüst, 185-191.

Hoyng, P. 1975, Thesis, University of Utrecht.

Hoyng, P. 1977, Astron. Astrophys. 55, 23-30.

Hoyng, P., Brown, J. C., and van Beek, H. F. 1976, Solar Phys. 48, 197-254.

Hudson, H. S. 1972, Solar Phys. 24, 414-428.

Kahler, S. 1971, Astrophys. J. 164, 365-368.

Kahler, S. 1975, Solar Gamma-, X-, and EUV Radiation, I.A.U. Symposium 68, Edited by S. Kane, D. Reidel Publishing Company, Dordrecht, 211-231.

Kane, S. R. 1973, High-Energy Phenomena on the Sun, Edited by R. Ramaty and R. G. Stone, NASA SP-342, 55-77.

Kane, S. R. 1974, Coronal Disturbances, I.A.U. Symposium 57, Edited by G. Newkirk, Jr., D. Reidel Publishing Company, Dordrecht, 105-141.

Kane, S. R. and Anderson, K. A. 1970, Astrophys. J. 162, 1003-1018.

Korchak, A. A. 1976, Sov. Astron. 20, 211-214; translated from Astron. Zh. 53, 370-376.

Kundu, M. R. 1965, Solar Radio Astronomy, Interscience Publishers, New York.

Mätzler, C. 1976, Solar Phys. 49, 117-140.

Mätzler, C., Bai, T., Crannell, C. J., and Frost, K. J. 1977, to be published (Paper 2).

Neupert, W. M. 1968, Astrophys. J. 153, L59-L64.

Peterson, L. E. and Winckler, J. R. 1959, J. Geophys. Res. 64, 697.

Ramaty, R. 1969, Astrophys. J. 158, 753-770.

Solar-Geophysical Data, Numbers 297 through 330, May 1969-February 1972, U. S. Department of Commerce, NOAA, (Boulder, Colorado, U. S. A. 80302).

Spicer, D. S. 1977, Solar Phys. 51, 431-434.

Spitzer, L. 1962, Physics of Fully Ionized Gases, Interscience, New York.

Takakura, T. 1973, High-Energy Phenomena on the Sun, Edited by R. Ramaty and R. G. Stone, NASA SP-342, 179-187.

Trubnikov, B. A. 1961, Phys. Fluids 4, 195-198.

Tucker, W. H. 1975, Radiation Processes in Astrophysics, The MIT Press, Cambridge.

Uralov, A. M. and Nefed'ev, V. P. 1976, Sov. Astron. 20, 590-592, Translated from Astron. Zh. 53, 1041-1045.

Vorpahl, J. A. and Takakura, T. 1974, Astrophys. J. 191, 563-565.

Wiehl, H. 1977, Solar Phys. (in press).

Zheleznyakov, V. V. 1970, Radio Emission of the Sun and Planets, Pergamon Press, New York.

Zirin, H. 1966, The Solar Atmosphere, Blaisdell Publishing Company, Waltham, p. 480.